J Nanostruct 10(3): 463-485, Summer 2020

RESEARCH PAPER

# Preparation and Characterization of NiO Based Nano-ceramic Composites as Alternative Anode Materials for Solid Oxide Fuel Cells (SOFCs)

***Devi Radhika and A Samson** **

*Department of Chemistry, Karunya Institute of Technology and Sciences, Karunya Nagar, India*

**ARTICLE INFO**

***Article History:***
*Received 21 February 2020*
*Accepted 08 April 2020*
*Published 01 July 2020*

***Keywords:***
*Alternate anode materials*
*Facile synthesis*
*Nano-ceramic composite materials*
*SOFC application*

**ABSTRACT**

Solid oxide fuel cell (SOFC) is being developed all over the world at present as a future energy conversion device. The alternative anode materials are also being studied in order to develop efficient low temperature SOFCs (LTSOFCs) operating below 800° C. Ni-based cermets are still the most promising anode materials and some targeted modifications are needed to improve the coking resistance and to enhance their electro-catalytic activity relatively at low temperature (~600 – 700 °C) range. Present work is aimed to develop alternate anode materials such as, NiO-$Ce_{0.9}Gd_{0.1}O_{2-\delta}$-$Ce_{0.9}Y_{0.1}O_{2-\delta}$, NiO-$Ce0_{.8}Gd_{0.2}O_{2-\delta}$-$Ce_{0.8}Y_{0.2}O_{2-\delta}$, NiO-$Ce_{0.9}Gd_{0.1}O_{2-\delta}$-$Ce_{0.9}Sm_{0.1}O_{2-\delta}$, NiO-$Ce_{0.8}Gd_{0.2}O_{2-\delta}$-$Ce_{0.8}Sm_{0.2}O_{2-\delta}$, NiO-$Ce_{0.9}Gd_{0.1}O_{2-\delta}$ and NiO-$Ce_{0.8}Gd_{0.2}O_{2-\delta}$ for by simple chemical precipitation route and characterize them towards application in SOFC systems. The precursor materials used in this synthesis were cerium nitrate hexahydrate, gadolinium nitrate, yttrium nitrate, samarium nitrate [as basic materials] and sodium hydroxide [as precipitator material]. C-TAB (cetyl trimethylammonium bromide) was used as a surfactant in order to avoid the agglomeration of the nanoparticles. The influence of Gd, Y and Sm doping on the phase structure development of ceria was investigated. The prepared anode materials were characterized by TGA, XRD, FTIR, particle size analysis, SEM and EDAX. The electrical characteristics of the materials were studied by electrochemical impedance spectroscopy. The results obtained were discussed in order to use the materials as alternate anode materials for SOFCs.

**How to cite this article**
*Radhika D and Nesaraj S. Preparation and Characterization of NiO Based Nano-ceramic Composites as Alternative Anode Materials for Solid Oxide Fuel Cells (SOFCs). J Nanostruct, 2020; 10(3):463-485. DOI: 10.22052/JNS.2020.03.004*

## INTRODUCTION

Solid oxide fuel cell (SOFC) is an electrochemical device that converts the energy of a chemical reaction directly into electrical energy. Recently, alternative anode materials have been proposed notably for low temperature SOFCs (LTSOFCs) operating below 800 °C. The role of an anode in SOFC is electro-oxidation of fuel by catalyzing the reaction, and facilitating fuel access and product removal. Therefore, the anode materials should meet certain requirements reported [1,2]: Stability in reducing environment, Sufficient electronic and ionic conductivity, Porous structure, Thermal expansion coefficient (TEC) matching with electrolyte materials, and High catalytic activity.

In SOFCs, anode is the place for the fuel oxidation with oxygen ions to generate $H_2O$ or $CO_2$. Of these, the most common SOFC anode is the Ni-

* *Corresponding Author Email: drsamson@karunya.edu*

based cermet, which exhibits a good compatibility with electrolytes, an excellent activity for hydrogen electro-oxidation and a sufficient electronic conductivity for electron transfer. However, when fed with hydrocarbons, quick carbon deposition over the Ni-based anode may be experienced due to the low coking resistance, and then, a quick cell performance degradation was observed. As a result, besides the development of new fuels for SOFCs, the rational design of the coking-resistant anodes is also important for the commercialization of hydrocarbon-fueled SOFCs. Recently, numerous efforts have been devoted to improve the coking resistance of hydrocarbon-fueled SOFCs, e.g., adopting perovskite-based anode materials, applying non-nickel-based anodes and modifying/ decorating the Ni-based cermet anodes [3]. The vast majority of SOFCs have a nickel anode because of its low cost compared to precious metals. The most frequently used anode materials are cermet composed of nickel and solid electrolyte, such as Ni-YSZ, Ni-SDC, targeting at maintaining porosity of anode by preventing sintering of the Ni particles and offering the anode with a TEC comparable to that of the solid electrolyte relatively lower temperature (600 $^{o}$C).

Yttria-doped ceria (YDC) and samaria-doped ceria (SDC) were proposed as potential anodes for intermediate temperature SOFCs [4,5]. The common feature of these two candidate materials is, in reducing atmosphere typical of anode environment, they exhibit characteristic of mixed ionic-electronic conductivity. Similar to Ni/YSZ cermet anode, Ni/doped ceria cermet has also been formulated and tested for use as potential anode in intermediate temperature SOFCs [6]. Nanocrystalline materials such as ZnO/NiO were proposed as alternate anode materials for LTSOFC operating below 500 °C [7]. It was found that nanocrystalline based anodes can exhibit good catalytic activity, high electronic and ionic conductivity in turn which may help to achieve high power output at reduced temperatures.

It was found that nanocrystalline based anodes can exhibit good catalytic activity, high electronic and ionic conductivity in turn which may help to achieve high power output. Yang Nai-Tao et al. have proposed new Ni-$Ce_{0.8}Gd_{0.2}O_{1.9}$ (CGO) cermet anodes for IT-SOFC application [8,9]. They found that NiO in the anodes can be reduced to Ni completely by the mixture of 20%$H_2$ ~ 80%He at 700 °C without the phase transformation of CGO. There are various processing routes for the synthesis of ceramic composite materials. Those routes include solid state route, sol-gel route, plasma spraying, laser synthesis, hydrothermal synthesis and co-precipitation route, green synthesis, combustion, microwave synthesis, thermal decomposition route, etc. [10-27]. In this research work, we report the preparation and characterization of a set of nanoceramic composite materials by a chemical precipitation route for application as alternate anode materials for SOFC systems.

## MATERIALS AND METHODS

### *Chemicals*

In this experiment, various chemicals have been used to prepare the nanocrystalline anode materials. The chemicals used and their details are presented in the Table 1. The aqueous solution containing a known amount of nickel nitrate, cerium nitrate, $Gd_2O_3$, $Sm_2O_3$/$Y_2O_3$ (as basic materials, dissolved in nitric acid) and sodium hydroxide (as precipitator material) was prepared in distilled water. Gadolinium nitrate, yttrium nitrate and samarium nitrate were prepared by dissolving the required quantity of $Gd_2O_3$, $Y_2O_3$ and $Sm_2O_3$ in $HNO_3$ respectively. The chemicals were taken for synthesis based on the stoichiometric calucation. The amount of precursor materials used for the preparation of different nanocrystalline materials are indicated in Table 2.

### *Materials synthesis*

Initially, the precipitating solution (sodium hydroxide) was mixed with 2 ml of 10% CTAB (as surfactant material). In order to avoid agglomeration this surfactant added to solution. To this mixture, $Ni(NO_3)_3$, $Ce(NO_3)_3$, $Gd(NO_3)_3$ and $Y(NO_3)_3$/$Sm(NO_3)_3$ solutions were subsequently added one by one drop wise. They were mixed thoroughly by a magnetic stirring apparatus (1,000 rpm) at room temperature for 2-3 hours under controlled alkaline pH range. The pH of the solution was adjusted in range of 11 – 14 by the addition of sodium hydroxide pellets[28,29]. The resultant precipitate ($(Ni(OH)_2$ + $Ce(OH)_4$ + $Gd(OH)_3$+ $Y(OH)_3$) or ($Ni(OH)_2$ + $Ce(OH)_4$ + $Gd(OH)_3$+ $Sm(OH)_3$ or ($Ni(OH)_2$ + $Ce(OH)_4$ + $Gd(OH)_3$) with CTAB was filtered and then washed with deionized water and ethanol in the ratio of 9:1 (v/v) five to ten times. The product was dried at 50 °C to 100 °C for 24 h. The resultant material was calcined at

Table 1. Details of required chemicals used for the preparation of anode nanocrystalline anode materials for SOFC application

| S.No. | Chemical name | Molecular formula | Molecular weight | Make | Purity/ Assay |
|---|---|---|---|---|---|
| 1 | Sodium hydroxide | NaOH | 40 | Merck | ≥ 97% |
| 2 | C-TAB (cetyl trimethyl ammonium bromide LR) | $C_{19}H_{42}BrN$ | 364.45 | SDFCL (S D Fine Chem Limited) India. | 98% |
| 3 | Cerium nitrate hexahydrate | $Ce(NO_3)_3.6H_2O$ | 434.2 | Himedia, India | 99% |
| 4 | Nickel nitrate hexahydrate | $Ni(NO_3)_3.6H_2O$ | 290.81 | Merck, India | ≥ 97% |
| 5 | Gadolinium oxide | $Gd_2O_3$ | 362.49 | Lobachemie, India | 99.9% |
| 6 | Yttrium oxide | $Y_2O_3$ | 225.81 | Lobachemie, India | 99.9% |
| 7 | Samarium oxide | $Sm_2O_3$ | 348.72 | Lobachemie, India | 99.9% |
| 8 | Nitric acid (70% pure) | $HNO_3$ | 63.01 | Merck, India | 68-72% |
| 9 | Ethanol (absolute) | $C_2H_5OH$ | 46.08 | Changshu Yangyuan Chemical, China | 99.9% |

300, 450, 600 and 750 °C for 2 hours each in air. During calcination, the surfactant was removed, and phase-pure nanocrystalline material was formed. The schematic representation of the synthesis of nanocrystalline materials by chemical precipitation method is shown in the Fig. 1.

*Reaction mechanisms involved*

The main reactions involved in the preparation of nanocrystalline ceramic composite oxide materials during the experimental procedure can be written briefly as follows:

*Reaction mechanisms involved*

The main reactions involved in the preparation of nanocrystalline ceramic composite oxide materials during the experimental procedure can be written briefly as follows:

*Reaction mechanism involved in the preparation of NiO-$Ce_{0.9}Gd_{0.1}O_{2-\delta}$ - $Ce_{0.9}Y_{0.1}O_{2-\delta}$*

$$7.8\ NaOH + 1.8\ Ce(NO_3)_3.6H_2O_{(aq)} + Ni(NO_3)_2 + 0.1\ Gd(NO_3)_3 + 0.1\ Y(NO_3)_3 \xrightarrow{H_2O} NiO - Ce_{0.9}Gd_{0.1}O_{2-\delta} - Ce_{0.9}Y_{0.1}O_{2-\delta_{(s)}} + 7.8\ NaNO_3\ (aq) + xH_2O_{(g)} \uparrow$$

*Reaction mechanism involved in the preparation of NiO-$Ce_{0.8}Gd_{0.2}O_{2-\delta}$ - $Ce_{0.8}Y_{0.2}O_{2-\delta}$*

$$7.6\ NaOH + 1.6\ Ce(NO_3)_3.6H_2O_{(aq)} + Ni(NO_3)_2 + 0.2\ Gd(NO_3)_3 + 0.2\ Y(NO_3)_3 \xrightarrow{H_2O} NiO - Ce_{0.8}Gd_{0.2}O_{2-\delta} - Ce_{0.8}Y_{0.2}O_{2-\delta_{(s)}} + 7.6\ NaNO_3\ (aq) + xH_2O_{(g)} \uparrow$$

*Reaction mechanism involved in the preparation of NiO-$Ce_{0.9}Gd_{0.1}O_{2-\delta}$ - $Ce_{0.9}Sm_{0.1}O_{2-\delta}$*

$$7.8\ NaOH + 1.8\ Ce(NO_3)_3.6H_2O_{(aq)} + Ni(NO_3)_2 + 0.1\ Gd(NO_3)_3 + 0.1\ Sm(NO_3)_3 \xrightarrow{H_2O} NiO - Ce_{0.9}Gd_{0.1}O_{2-\delta} - Ce_{0.9}Sm_{0.1}O_{2-\delta_{(s)}} + 7.8\ NaNO_3\ (aq) + xH_2O_{(g)} \uparrow$$

*Reaction mechanism involved in the preparation of NiO-$Ce_{0.8}Gd_{0.2}O_{2-\delta}$ - $Ce_{0.8}Sm_{0.2}O_{2-\delta}$*

Table 2. Amount of precursor materials (dissolved in 100 ml of water each) used for the preparation of ceria based anode nanocrystalline ceramic composite materials by chemical precipitation method

| Sample | Concentration of $Ni(NO_3)_2$/ Wt.(g) | Concentration of $Ce(NO_3)_3$ / Wt. (g) | Concentration of $Gd(NO_3)_3$ / Wt. $Gd_2O_3$ (g) | Concentration of $Y(NO_3)_3$ / Wt. $Y_2O_3$ (g) | Concentration of $Sm(NO_3)_3$ / Wt. $Sm_2O_3$ (g) | Concentration of NaOH / Wt. (g) |
|---|---|---|---|---|---|---|
| $NiO-Ce_{0.9}Gd_{0.1}O_{2-\delta}$ - $Ce_{0.9}Y_{0.1}O_{2-\delta}$ | 0.1 M / 2.908 g | 0.18 M / 7.815 g | 0.01 M / 0.181 g | 0.01 M / 0.112 g | ---- | 0.78 M / 3.12 g |
| $NiO-Ce_{0.8}Gd_{0.2}O_{2-\delta}$ - $Ce_{0.8}Y_{0.2}O_{2-\delta}$ | 0.1 M / 2.908 g | 0.16 M / 69.47 g | 0.02 M / 0.363 g | 0.02 M / 0.225 g | ---- | 0.76 M / 3.04 g |
| $NiO-Ce_{0.9}Gd_{0.1}O_{2-\delta}$ - $Ce_{0.9}Sm_{0.1}O_{2-\delta}$ | 0.1 M / 2.908 g | 0.18 M / 7.815 g | 0.01 M / 0.181 g | ---- | 0.1 M / 1.74 g | 0.78 M / 3.12 g |
| $NiO-Ce_{0.8}Gd_{0.2}O_{2-\delta}$ - $Ce_{0.8}Sm_{0.2}O_{2-\delta}$ | 0.1 M / 2.908 g | 0.16 M / 6.947 g | 0.02 M / 0.363 g | ---- | 0.2 M / 3.48 g | 0.76 M / 3.04 g |
| $NiO-Ce_{0.9}Gd_{0.1}O_{2-\delta}$ | 0.1 M / 2.908 g | 0.09 M / 3.907 g | 0.01 M / 0.181 g | ---- | ---- | 0.39 M / 1.52 g |
| $NiO-Ce_{0.8}Gd_{0.2}O_{2-\delta}$ | 0.1 M / 2.908 g | 0.08 M / 3.473 g | 0.02 M / 0.181 g | ---- | ---- | 0.38 M / 1.44 g |

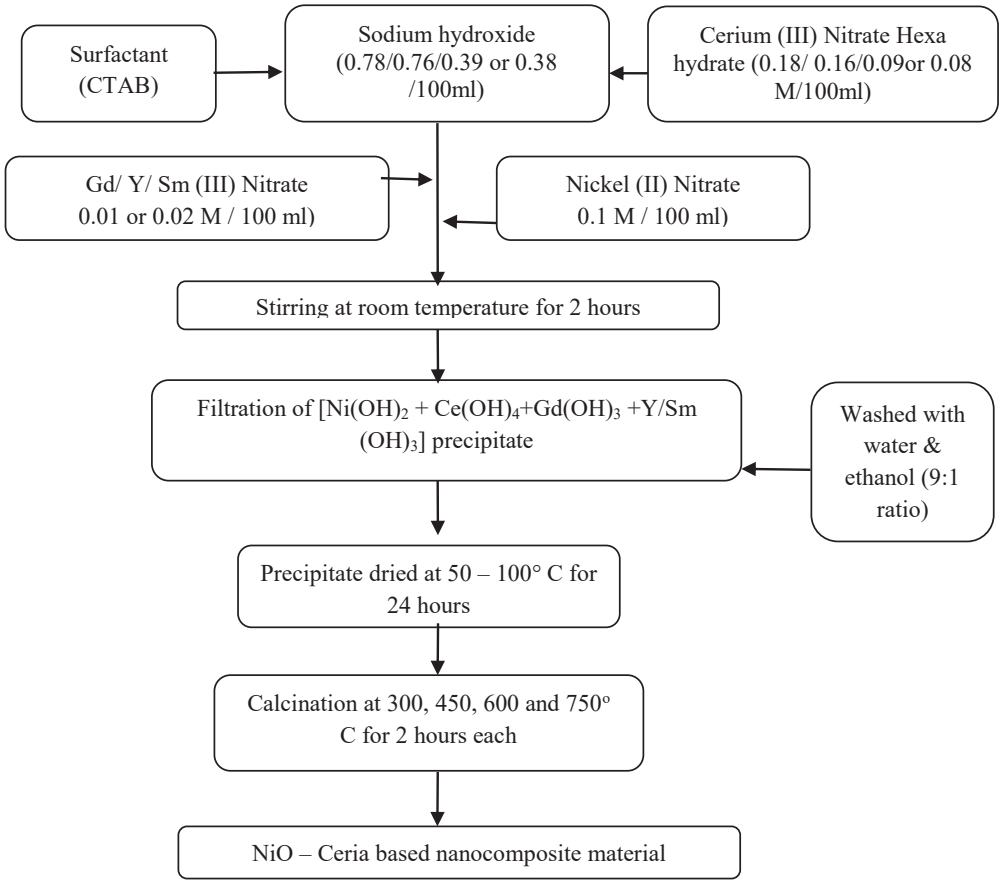


Fig. 1. Schematic representation of the synthesis of nanocrystalline materials by chemical precipitation method

$$7.6\ NaOH + 1.6\ Ce(NO_3)_3.6H_2O_{(aq)} + Ni(NO_3)_2 + 0.2\ Gd(NO_3)_3 + 0.2\ Sm(NO_3)_3 \xrightarrow{H_2O} NiO - Ce_{0.8}Gd_{0.2}O_{2-\delta} - Ce_{0.8}Sm_{0.2}O_{2-\delta(s)} + 7.6\ NaNO_3\ (aq) + xH_2O_{(g)} \uparrow$$

*Reaction mechanism involved in the preparation of NiO-$Ce_{0.9}Gd_{0.1}O_{2-\delta}$*

$$3.9\ NaOH + 0.9\ Ce(NO_3)_3.6H_2O_{(aq)} + Ni(NO_3)_2 + 0.1\ Gd(NO_3)_3 + \xrightarrow{H_2O} NiO - Ce_{0.9}Gd_{0.1}O_{2-\delta(s)} + 3.9\ NaNO_3\ (aq) + xH_2O_{(g)} \uparrow$$

*Reaction mechanism involved in the preparation of NiO-$Ce_{0.8}Gd_{0.2}O_{2-\delta}$*

$$3.8\ NaOH + 0.8\ Ce(NO_3)_3.6H_2O_{(aq)} + Ni(NO_3)_2 + 0.\ Gd(NO_3)_3 + \xrightarrow{H_2O} NiO - Ce_{0.8}Gd_{0.2}O_{2-\delta(s)} + 3.8\ NaNO_3\ (aq) + xH_2O_{(g)}$$

*Characterizations*

The precursor samples were subjected to thermo gravimetric analysis experiments with Perkin Elmer TGA 7 instrument to know about the temperature of formation of phase pure materials. The heat treated powder was characterized by Shimadzu XRD6000 X-ray diffractometer using CuKα radiation. The lattice parameters were

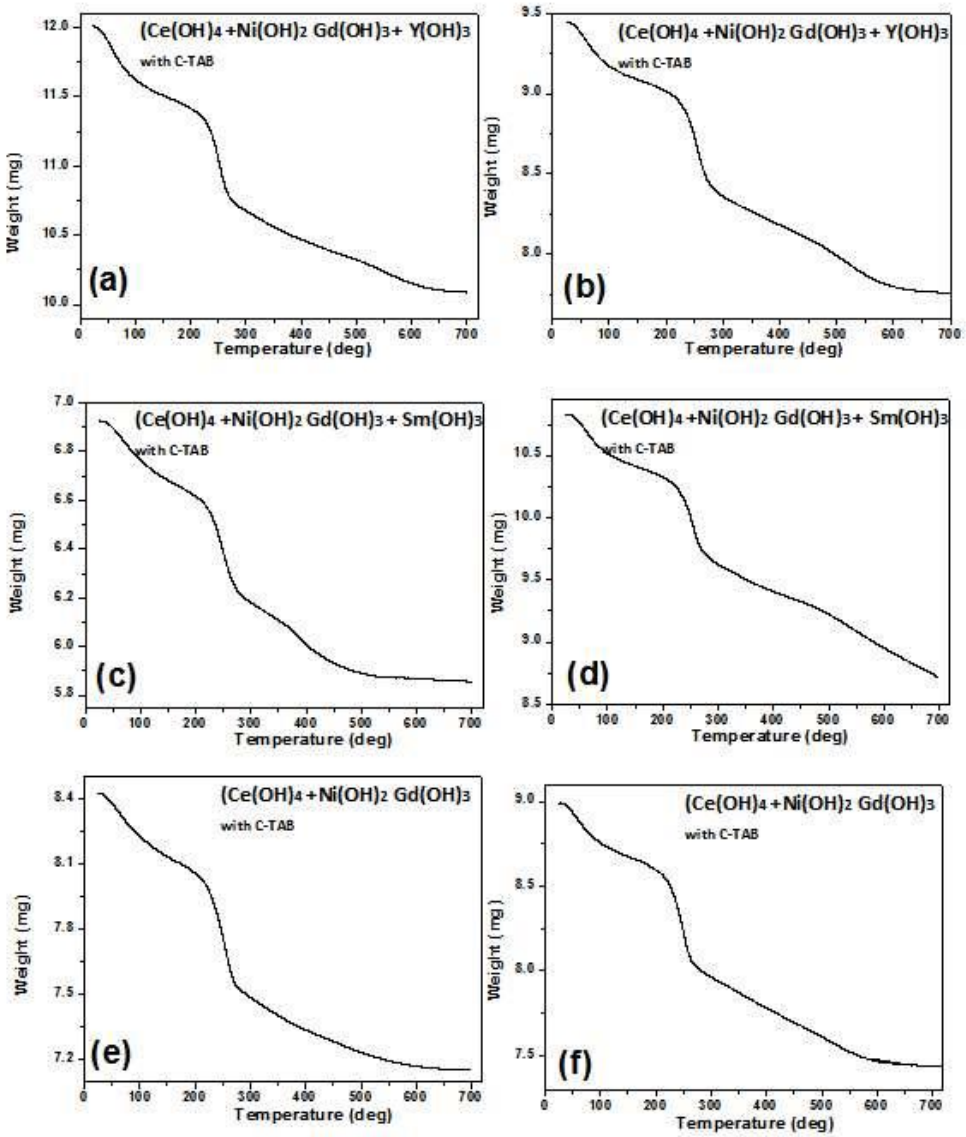


Fig. 2. (a, b, c, d & e). TGA spectra obtained with the NiO-based doped ceria precursor materials (a) NiO-$Ce_{0.9}Gd_{0.1}O_{2-\delta}$-$Ce_{0.9}Y_{0.1}O_{2-\delta}$, (b) NiO-$Ce0_{.8}Gd_{0.2}O_{2-\delta}$-$Ce_{0.8}Y_{0.2}O_{2-\delta}$, (c) NiO-$Ce_{0.9}Gd_{0.1}O_{2-\delta}$-$Ce_{0.9}Sm_{0.1}O_{2-\delta}$, (d) NiO-$Ce_{0.8}Gd_{0.2}O_{2-\delta}$-$Ce_{0.8}Sm_{0.2}O_{2-\delta}$, (e) NiO-$Ce_{0.9}Gd_{0.1}O_{2-\delta}$ and (f) NiO-$Ce_{0.8}Gd_{0.2}O_{2-\delta}$

Table 3. Thermo gravimetric analysis data obtained on precursor materials

| Sample | Initial weight (mg) at 25°C | Final weight (mg) at 700°C | Total weight loss (mg) | Total Weight loss (%) |
|---|---|---|---|---|
| NiO-$Ce_{0.9}Gd_{0.1}O_{2-\delta}$-$Ce_{0.9}Y_{0.1}O_{2-\delta}$ | 12.00 | 10.08 | 1.2 | 13% |
| NiO-$Ce_{0.8}Gd_{0.2}O_{2-\delta}$-$Ce_{0.8}Y_{0.2}O_{2-\delta}$ | 9.45 | 7.76 | 1.69 | 17% |
| NiO-$Ce_{0.9}Gd_{0.1}O_{2-\delta}$-$Ce_{0.9}Sm_{0.1}O_{2-\delta}$ | 6.92 | 5.85 | 1.07 | 11% |
| NiO-$Ce_{0.8}Gd_{0.2}O_{2-\delta}$-$Ce_{0.8}Sm_{0.2}O_{2-\delta}$ | 10.83 | 8.70 | 2.13 | 22% |
| NiO-$Ce_{0.9}Gd_{0.1}O_{2-\delta}$ | 8.42 | 7.15 | 1.27 | 13% |
| NiO-$Ce_{0.8}Gd_{0.2}O_{2-\delta}$ | 8.99 | 7.43 | 1.56 | 16% |

calculated by least square fitting method using DOS computer programming. The theoretical density of the powders was calculated with the obtained XRD data. The crystallite sizes of the powder were calculated by Scherrer's formula. JASCO FTIR spectrometer was employed to record the FTIR spectra of materials in the range of 4000 – 400 $cm^{-1}$. The surface morphology of the particles was studied by means of JEOL Model JSM-6360 scanning electron microscope. EDAX analysis was also performed with JEOL Model JSM-6360 to find out the percentage of elements present in the samples. The particle size of the powder was measured using Malvern Particle Size Analyzer using triple distilled water as medium.

The circular pellets (8 mm diameter x 1.5 mm thickness) were prepared from the materials by applying a pressure of 1.2 ton with a mini hydraulic pelletizer. They were sintered at 700° C for 3 hours and finally subjected to high temperature electrochemical impedance spectroscopy studies. The complex impedance spectroscopy measurements have carried out using a Solatron 1260 frequency response analyzer (FRA) combined with Solatron 1296 electrochemical interface (ECI).

## RESULTS AND DISCUSSION

*Thermogravimetric analysis*

The dried precursor precipitate samples [($Ni(OH)_2$ + $Ce(OH)_4$ + $Gd(OH)_3$ + $Y(OH)_3$, $Ni(OH)_2$ + $Ce(OH)_4$ + $Gd(OH)_3$ + $Sm(OH)_3$ and $Ni(OH)_2$ + $Ce(OH)_4$ + $Gd(OH)_3$) with C-TAB,] with an initial mass 6-12 mg was placed in an open platinum crucible. The TGA patterns obtained with the precursor precipitate materials are indicated in Fig. 2 (a, b, c, d, e & f).

From the figures, it was understood the total weight loss was found to be in the range of various percentage levels from the temperature of 25 to 700 °C. From the curve, it was understood that the weight loss begins to appear from the initial stage itself. From the curves the thermal decomposition of the molecule can be divided into four separate regions as explained in the literature [30]. The thermo gravimetric analysis data obtained on the precursor materials is presented in Table 3.

From the curves, it was found that, the weight loss of about 2% is found at around 100 °C, which may be due to the removal of water molecule from the sample. Then, the total weight loss of 5-6% is found at around 250 °C in all the samples, which may be attributed to the phase formation of NiO in the sample [30]. The further weight loss present in the sample until 700 °C is due to the decomposition of remaining carbon/nitrogen-based compounds from the sample. At around 700 °C, the weight loss is stable, which indicates the formation of phase-pure ceramic oxide materials. The total weight loss of about 11-22% is found in all the samples.

*Structural analysis by X-ray Diffraction studies*

The XRD patterns of the nanocrystalline ceramic composite oxide materials prepared by the chemical precipitation method with CTAB as surfactant are shown in Fig. 3. The XRD patterns of the calcined NiO based nanocrystalline ceramic composite oxide powders reveal the formation of well-crystallined single-phase materials.

The XRD patterns obtained on these materials were compared with the standard data for NiO (JCPDS card No. 75-0197) [31] and ceria (JCPDS card No. 81-0792) [32]. The lattice parameters, the theoretical density ($D_X$) and Crystallite size of the samples were calculated as shown in Table 4.

The x-ray broadening provides information about crystallite size by Debye- Scherrer equation. Crystallite size of the samples was calculated from

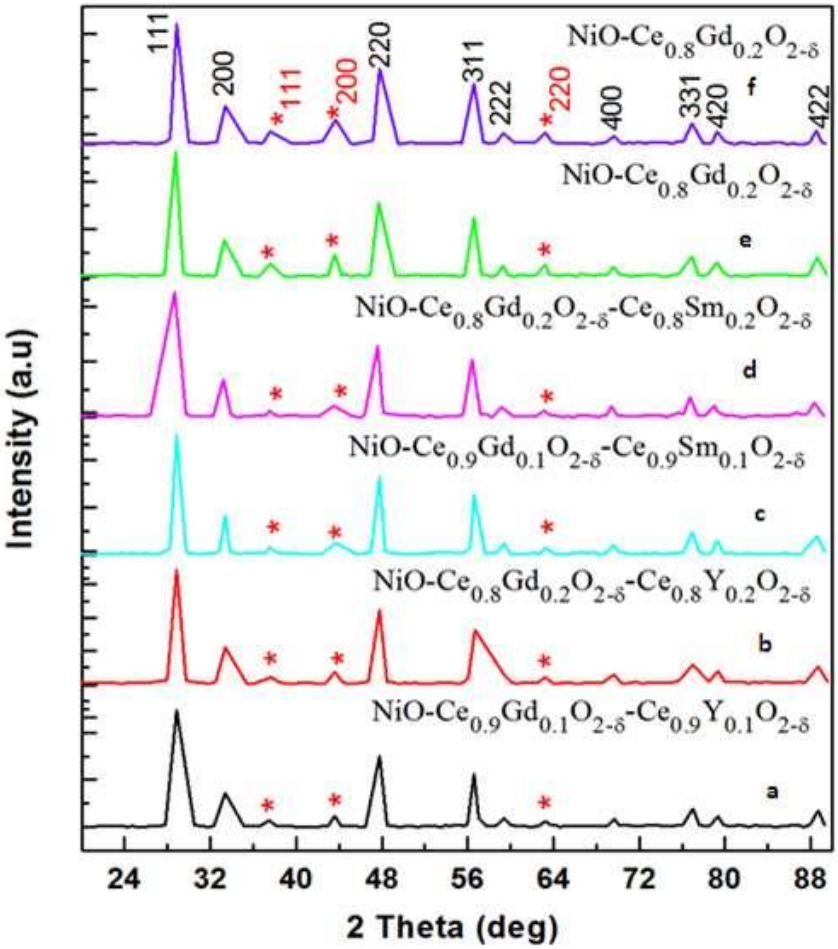


Fig. 3. XRD pattern obtained on (a) NiO-$Ce_{0.9}Gd_{0.1}O_{2-\delta}$-$Ce_{0.9}Y_{0.1}O_{2-\delta}$, (b) NiO-$Ce0_{.8}Gd_{0.2}O_{2-\delta}$-$Ce_{0.8}Y_{0.2}O_{2-\delta}$, (c) NiO-$Ce_{0.9}Gd_{0.1}O_{2-\delta}$-$Ce_{0.9}Sm_{0.1}O_{2-\delta}$, (d) NiO-$Ce_{0.8}Gd_{0.2}O_{2-\delta}$-$Ce_{0.8}Sm_{0.2}O_{2-\delta}$, (e) NiO-$Ce_{0.9}Gd_{0.1}O_{2-\delta}$ and (f) NiO-$Ce_{0.8}Gd_{0.2}O_{2-\delta}$ nanocrystalline ceramic composite oxide powder

XRD line broadening method using the following Scherrer relationship (Equation 1).

$$D_p = \frac{k\lambda}{\beta \cos\theta} \quad (1)$$

Where '$D_p$' is the crystallite size in nm, 'k' is a numerical constant (~0.9), 'λ' is the wavelength of X-rays (for Cu Kα radiation, λ = 1.5418 Å), 'β' is the effective broadening taken as a full width at half maximum (FWHM) (in radians), 'θ' is the diffraction angle for the peak.

The lattice parameters are calculated from 2θ values in the X-ray diffraction patterns by using DOS computer programming. The theoretical density ($D_x$) for the samples was calculated according to the formula (Equation 2).

$$D_x = \frac{Z \times M}{N \times V}\ g.cm^{-3} \quad (2)$$

Where, Z = number of chemical species in the unit cell, M = molecular mass of the sample (g/mol), N = Avogadro's number (6.022 x $10^{23}$) and V is the volume of the crystalline unit cell as determined by x-ray diffraction.

The XRD patterns of the heat-treated NiO based ceria based ceramic composite oxide powders reveal the formation of well-crystallined materials with cubic fluorite structure geometry [33-35]. No impurity peaks were observed in the XRD patterns of all the nanocrystalline materials. The crystallographic planes observed at (111), (200), (220), (311), (222), (400), (331), (420) and (422) as per JCPDS No: 81-0792 are indicated in $CeO_2$ phase [32]. The crystallographic planes observed at (111), (200) and (220) as per JCPDS No: 75-0197 are indicated in NiO phase [31].

Table 4. Crystallographic parameters obtained on the NiO-based ceria-doped nano composite materials

| Sample | Crystallite structure | $CeO_2$ phase (JCPDS No. 81-0792) | | | NiO phase (JCPDS No. 75-0792) | | | Crystallite size |
|---|---|---|---|---|---|---|---|---|
| | | Unit cell parameter 'a' (Å) | Unit cell volume ($Å^3$) | Theoretical density (g/cc) | Unit cell parameter 'a' (Å) | Unit cell volume ($Å^3$) | Theoretical density (g/cc) | |
| JCPDS data for ceria and NiO phase | Cubic (F.C.C) | 5.412 | 158.516 | 7.211 | 4.170 | 72.511 | 6.843 | --- |
| NiO-$Ce_{0.9}Gd_{0.1}O_{2-\delta}$-$Ce_{0.9}Y_{0.1}O_{2-\delta}$ | Cubic (F.C.C) | 5.398 | 157.289 | 7.161 | 4.158 | 71.887 | 6.900 | 20.1 |
| NiO-$Ce_{0.8}Gd_{0.2}O_{2-\delta}$-$Ce_{0.8}Y_{0.2}O_{2-\delta}$ | Cubic (F.C.C) | 5.397 | 157.201 | 7.127 | 4.155 | 71.732 | 6.915 | 18.6 |
| NiO-$Ce_{0.9}Gd_{0.1}O_{2-\delta}$-$Ce_{0.9}Sm_{0.1}O_{2-\delta}$ | Cubic (F.C.C) | 5.401 | 157.551 | 7.697 | 4.155 | 71.732 | 6.915 | 16.7 |
| NiO-$Ce_{0.8}Gd_{0.2}O_{2-\delta}$-$Ce_{0.8}Sm_{0.2}O_{2-\delta}$ | Cubic (F.C.C) | 5.412 | 158.516 | 8.139 | 4.161 | 72.043 | 6.885 | 20.8 |
| NiO-$Ce_{0.9}Gd_{0.1}O_{2-\delta}$ | Cubic (F.C.C) | 5.402 | 157.639 | 7.289 | 4.158 | 71.887 | 6.900 | 16.6 |
| NiO-$Ce_{0.8}Gd_{0.2}O_{2-\delta}$ | Cubic (F.C.C) | 5.403 | 157.726 | 7.391 | 4.154 | 71.680 | 6.920 | 19.5 |

*FTIR Studies*

Fig. 4 (a, b, c, d, e & f) shows the FTIR spectra obtained on NiO based ceria nanocrystalline ceramic composite oxide materials prepared by the chemical precipitation method. FTIR measurements were done using KBr method at room temperature (RT).

As seen from the spectra, only a prominent peak ~400 $cm^{-1}$ is found. This peak represents to Ni-O stretching vibrations reported earlier [36]. It is reported that pure $CeO_2$ has shown a broad band at 1383 $cm^{-1}$ [37]. In our study, all the samples have shown the characteristic peak of $CeO_2$ exactly at 1383.6 $cm^{-1}$. The samples showed peaks at around 2360 $cm^{-1}$, which may be due to the presence of dissolved or atmospheric $CO_2$ in the sample [37]. The peak appeared at 1600 $cm^{-1}$ is attributable to H-O-H bending mode and is indicative of the presence of molecular water in the samples [37]. The wide absorption bands that appeared in the spectra nearly at 3400 $cm^{-1}$ are attributed to the stretching vibration of water H-O bond (moisture) [37]. The absorption of atmospheric $CO_2$ and water molecule is common in $CeO_2$ based materials [38]. The bands in the region 1,000 to 650 $cm^{-1}$ have been assigned to the stretching modes, and the region 650 to 450 $cm^{-1}$ contains bridging stretching modes in the samples [39]. The important peaks observed from FTIR spectra assigned for characteristic peaks have shown in the Table 5.

*Particle size measurements*

The particle size distribution curves of NiO-based nanocrystalline ceramic composite oxide materials are shown in Fig. 5. For all the measurements, the sample is sonicated with triple distilled water for about 10 minutes and after that the sample is subjected for particle size analysis. Particle characteristics data (based on volume) obtained with NiO-based nanocrystalline ceramic composite oxide powders prepared by chemical precipitation method is indicated in Table 6.

From the Figures and the particle characteristics data (Table 6) it is observed that the samples size present between the diameters of 166-230 nm range. And also, it was noticed that both nano and micro particles present in all the samples. The presence of larger particles with micron size may be due to the high temperature treatment. It was reported that the particles may agglomerate when they subject to high temperature calcination process [40].

*Morphological studies by Scanning Electron Microscope (SEM)*

The SEM pictures obtained on NiO-based nanocrystalline ceramic composite oxide powders (NiO-$Ce_{0.9}Gd_{0.1}O_{2-\delta}$-$Ce_{0.9}Y_{0.1}O_{2-\delta}$, NiO-$Ce0_{.8}Gd_{0.2}O_{2-\delta}$-$Ce_{0.8}Y_{0.2}O_{2-\delta}$, NiO-$Ce_{0.9}Gd_{0.1}O_{2-\delta}$-$Ce_{0.9}Sm_{0.1}O_{2-\delta}$, NiO-$Ce_{0.8}Gd_{0.2}O_{2-\delta}$-$Ce_{0.8}Sm_{0.2}O_{2-\delta}$, NiO-$Ce_{0.9}Gd_{0.1}O_{2-\delta}$ and NiO-$Ce_{0.8}Gd_{0.2}O_{2-\delta}$) calcined at 750 °C are

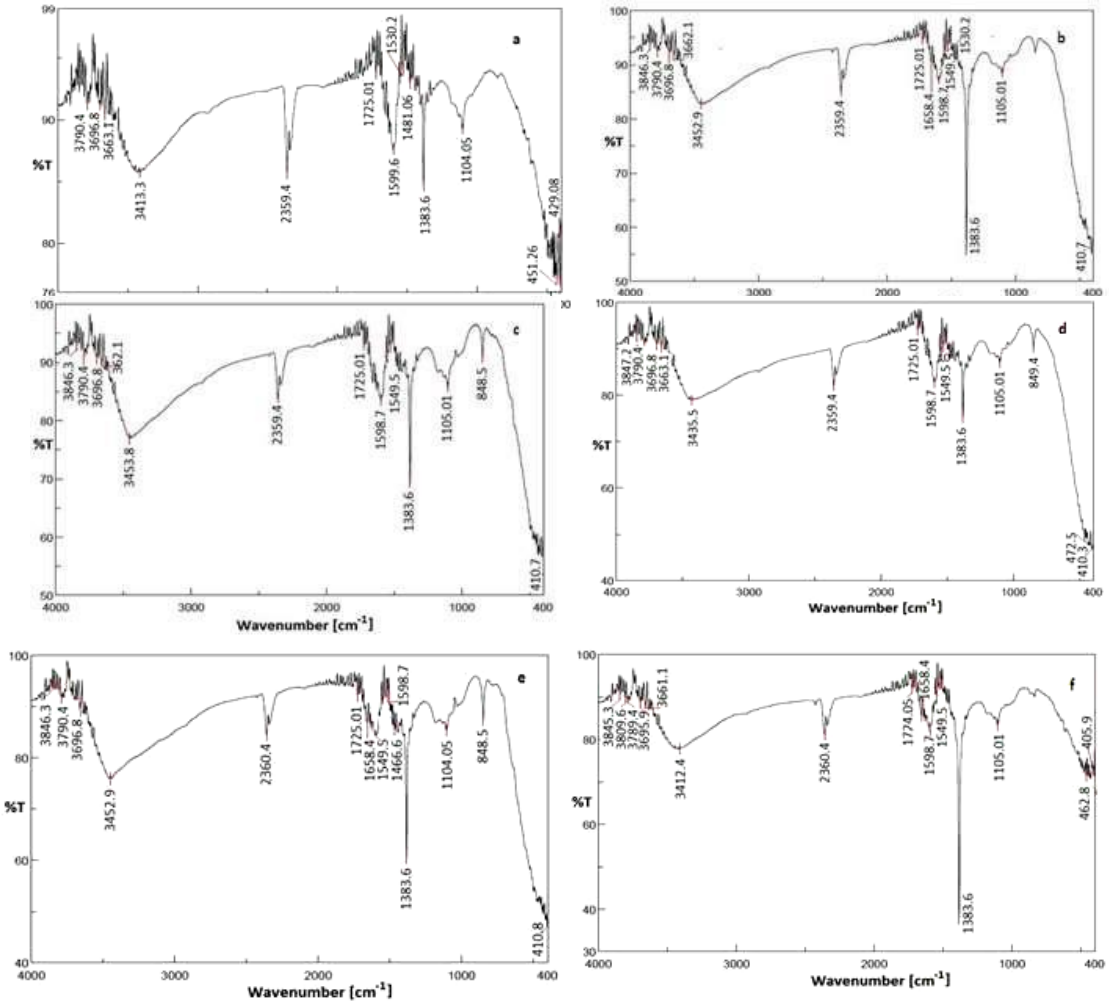


Fig. 4. FTIR spectra obtained on (a) NiO-$Ce_{0.9}Gd_{0.1}O_{2-\delta}$-$Ce_{0.9}Y_{0.1}O_{2-\delta}$, (b) NiO-$Ce0_{.8}Gd_{0.2}O_{2-\delta}$-$Ce_{0.8}Y_{0.2}O_{2-\delta}$, (c) NiO-$Ce_{0.9}Gd_{0.1}O_{2-\delta}$-$Ce_{0.9}Sm_{0.1}O_{2-\delta}$, (d) NiO-$Ce_{0.8}Gd_{0.2}O_{2-\delta}$-$Ce_{0.8}Sm_{0.2}O_{2-\delta}$, (e) NiO-$Ce_{0.9}Gd_{0.1}O_{2-\delta}$ and (f) NiO-$Ce_{0.8}Gd_{0.2}O_{2-\delta}$ nanocrystalline ceramic composite oxide powder

shown in Figs. 6-11 (a & b) respectively. For all the nanocomposite ceramic oxide powders, SEM photographs have taken at two resolutions, such as, 10,000 and 30,000.

The morphology of the NiO-based nanocrystalline ceramic composite oxide powders revealed that the particles exhibit spherical shape and the size of these particles shown around 100 nm. From the pictures it is observed that, there are some micro particles also presented. These particles are formed from nano particles due to agglomeration and look like micro particles [40]. The addition of surfactant (CTAB) prevented the possibility of high agglomeration and helped to get fine nanocrystalline powders.

*EDAX Analysis*

The EDAX spectra obtained with nanocrystalline ceramic composite oxide powders are reported in Fig. 12.

The chemical composition data observed for the samples from the EDAX analysis is indicated in Table 7. From the data, it was found that the elements were present as per the necessity.

*Conductivity studies*

Doped ceria has emerged as an alternate material for SOFC. Ceria exhibits mixed ionic and electronic conductivity in reducing atmospheres. Doping with rare earth metals, like gadolinium, increases its stability and conductivity. The relative high values for ionic conduction were

Table 5. Assignment of important peaks obtained from FTIR spectra of NiO- based nanocrystalline ceramic composite oxide powders

| Sample | Assignment of characteristic peaks ($cm^{-1}$) | | | | |
|---|---|---|---|---|---|
| | $CeO_2$ | Ni-O | Atmospheric $CO_2$ | H-O-H bending | H-O stretching bond |
| Reference Peaks [15,19] | 1383 | Near 400 | 2360 | 1600 | 3400 |
| $NiO\text{-}Ce_{0.9}Gd_{0.1}O_{2-\delta}\text{-}Ce_{0.9}Y_{0.1}O_{2-\delta}$ | 1383.6 | 408.3 | 2359.4 | 1599.6 | 3437.4 |
| $NiO\text{-}Ce_{0.8}Gd_{0.2}O_{2-\delta}\text{-}Ce_{0.8}Y_{0.2}O_{2-\delta}$ | 1383.6 | 410.7 | 2360.4 | 1598.7 | 3433.6 |
| $NiO\text{-}Ce_{0.9}Gd_{0.1}O_{2-\delta}\text{-}Ce_{0.9}Sm_{0.1}O_{2-\delta}$ | 1383.6 | 410.7 | 2360.4 | 1598.7 | 3408.5 |
| $NiO\text{-}Ce_{0.8}Gd_{0.2}O_{2-\delta}\text{-}Ce_{0.8}Sm_{0.2}O_{2-\delta}$ | 1383.6 | 410.3 | 2360.4 | 1598.7 | 3432.6 |
| $NiO\text{-}Ce_{0.9}Gd_{0.1}O_{2-\delta}$ | 1383.6 | 410.8 | 2360.4 | 1598.7 | 3453.8 |
| $NiO\text{-}Ce_{0.8}Gd_{0.2}O_{2-\delta}$ | 1383.6 | 405.9 | 2360.4 | 1598.7 | 3451.9 |

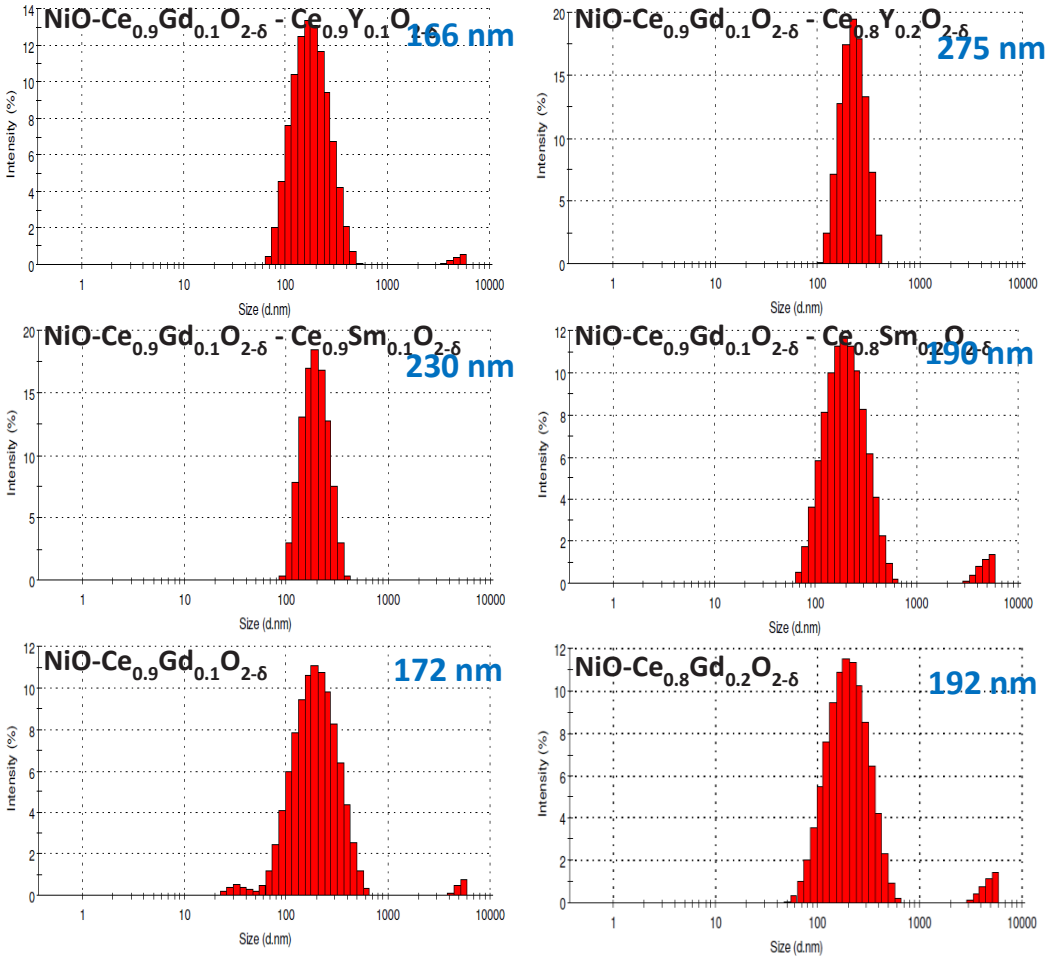


Fig. 5. Particle size curves obtained on nanocrystalline ceramic composite oxide powders

observed with Sm, Gd and Y as acceptor dopants [41]. Considering the abundance of these rare-earth elements, rare earth doped ceria used as a potentially low-cost electrolyte for IT-SOFC. Recently, mixed ionic electronic conductivity (MIEC) anode materials such as NiO-GDC, NiO-

Table 6. Particle characteristic data (based on volume) obtained with NiO- based nano crystalline ceramic composite oxide powders

| Sample | Peak 1 | | | Peak 2 | | | Avg. particle size (nm) |
|---|---|---|---|---|---|---|---|
| | Size (d.nm) | Intensity (%) | Width (d.nm) | Size (d.nm) | Intensity (%) | Width (d.nm) | |
| NiO-$Ce_{0.9}Gd_{0.1}O_{2-\delta}$-$Ce_{0.9}Y_{0.1}O_{2-\delta}$ | 189.3 | 98.8 | 76.88 | 4991 | 1.2 | 612.2 | 166.3 |
| NiO-$Ce_{0.8}Gd_{0.2}O_{2-\delta}$-$Ce_{0.8}Y_{0.2}O_{2-\delta}$ | 228.9 | 100 | 62.52 | --- | --- | --- | 275.5 |
| NiO-$Ce_{0.9}Gd_{0.1}O_{2-\delta}$-$Ce_{0.9}Sm_{0.1}O_{2-\delta}$ | 197.7 | 100 | 57.71 | --- | --- | --- | 230.3 |
| NiO-$Ce_{0.8}Gd_{0.2}O_{2-\delta}$-$Ce_{0.8}Sm_{0.2}O_{2-\delta}$ | 213.6 | 96.1 | 96.73 | 4713 | 3.9 | 773.1 | 190.4 |
| NiO-$Ce_{0.9}Gd_{0.1}O_{2-\delta}$ | 213.3 | 96.7 | 102.2 | 35.4 | 2 | 7.619 | 172.4 |
| NiO-$Ce_{0.8}Gd_{0.2}O_{2-\delta}$ | 214.2 | 96.2 | 97.9 | 4774 | 3.8 | 735.9 | 191.2 |

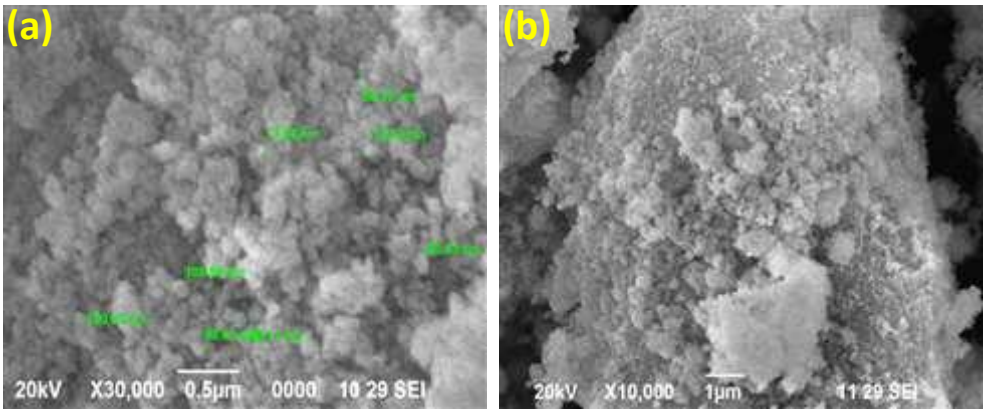


Fig. 6. (a & b) SEM photographs obtained on NiO-$Ce_{0.9}Gd_{0.1}O_{2-\delta}$-$Ce_{0.9}Y_{0.1}O_{2-\delta}$ powder in two different magnifications (a) 30,000 and (b) 10,000

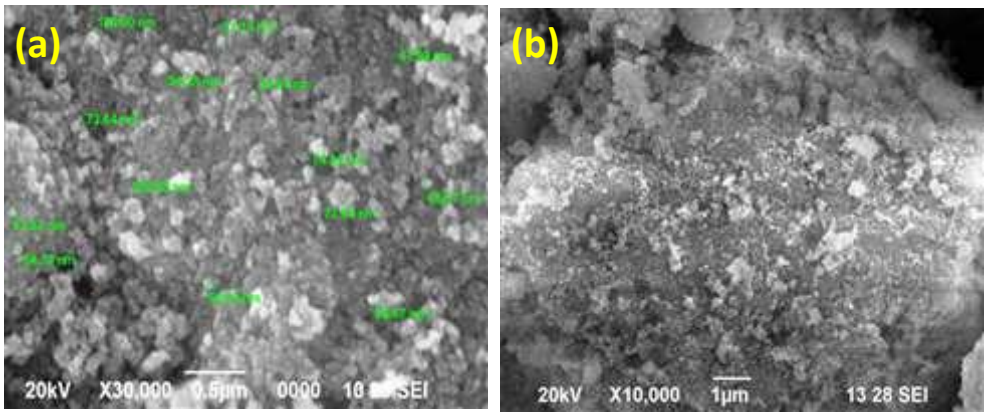


Fig. 7. (a & b) SEM photographs obtained on NiO-$Ce_{0.8}Gd_{0.2}O_{2-\delta}$-$Ce_{0.8}Y_{0.2}O_{2-\delta}$ powder in two different magnifications (a) 30,000 and (b) 10,000

SDC, etc. are proposed for SOFC application [40-41]. Therefore our proposed nanocrystalline ceramic composite oxide materials were subjected to electrical conductivity measurements as per the

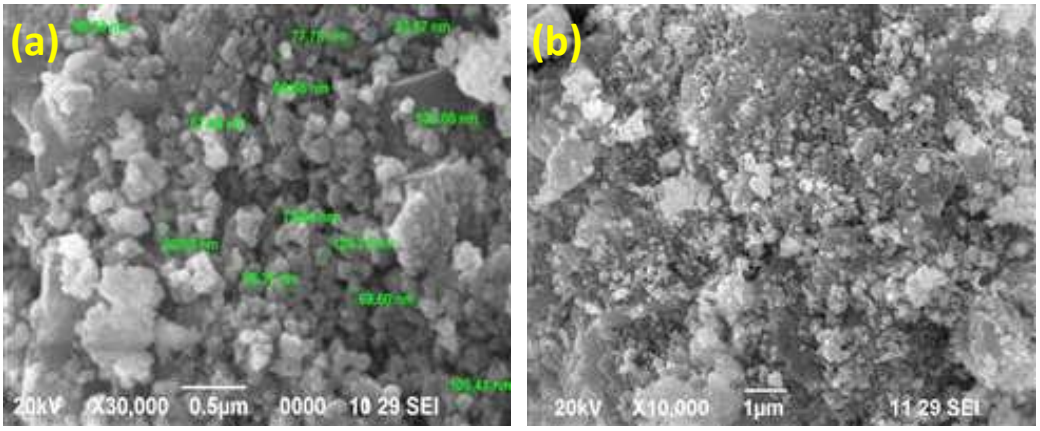


Fig. 8. (a & b) SEM photographs obtained on NiO-$Ce_{0.9}Gd_{0.1}O_{2-\delta}$-$Ce_{0.9}Sm_{0.1}O_{2-\delta}$ powder in two different magnifications (a) 30,000 and (b) 10,000

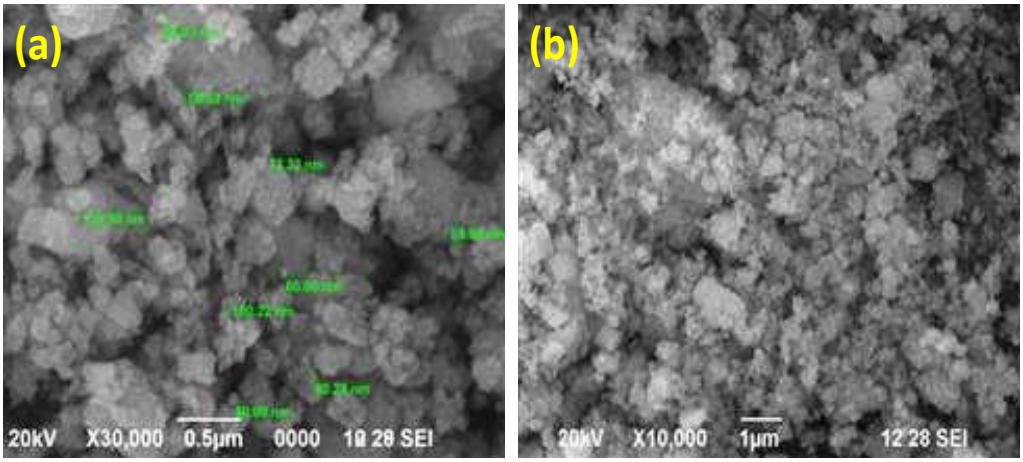


Fig. 9. (a & b) SEM photographs obtained on NiO-$Ce_{0.8}Gd_{0.2}O_{2-\delta}$-$Ce_{0.8}Sm_{0.2}O_{2-\delta}$ powder in two different magnifications (a) 30,000 and (b) 10,000

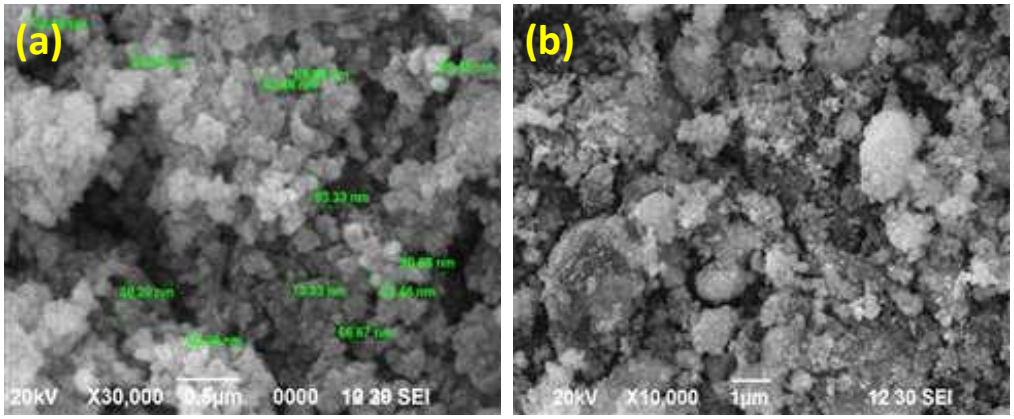


Fig.10. (a & b) SEM photographs obtained on NiO-$Ce_{0.9}Gd_{0.1}O_{2-\delta}$ ceramic powder in two different magnifications (a) 30,000 and (b) 10,000

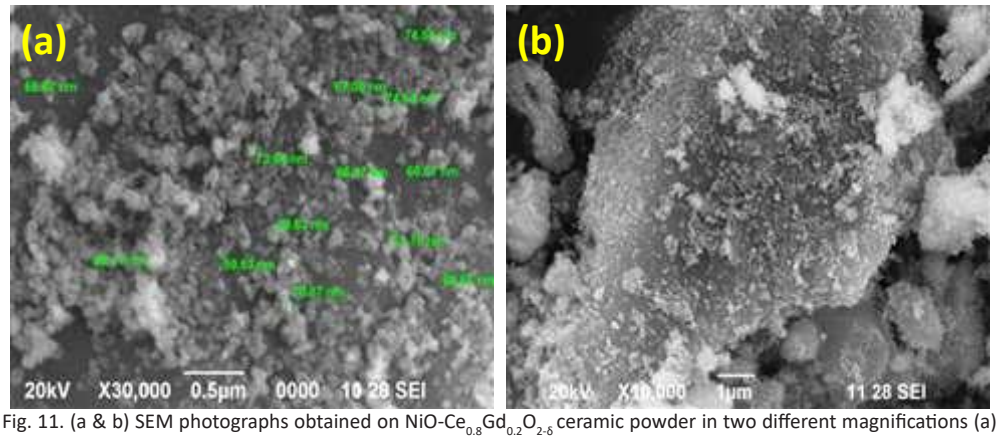


Fig. 11. (a & b) SEM photographs obtained on NiO-$Ce_{0.8}Gd_{0.2}O_{2-\delta}$ ceramic powder in two different magnifications (a) 30,000 and (b) 10,000

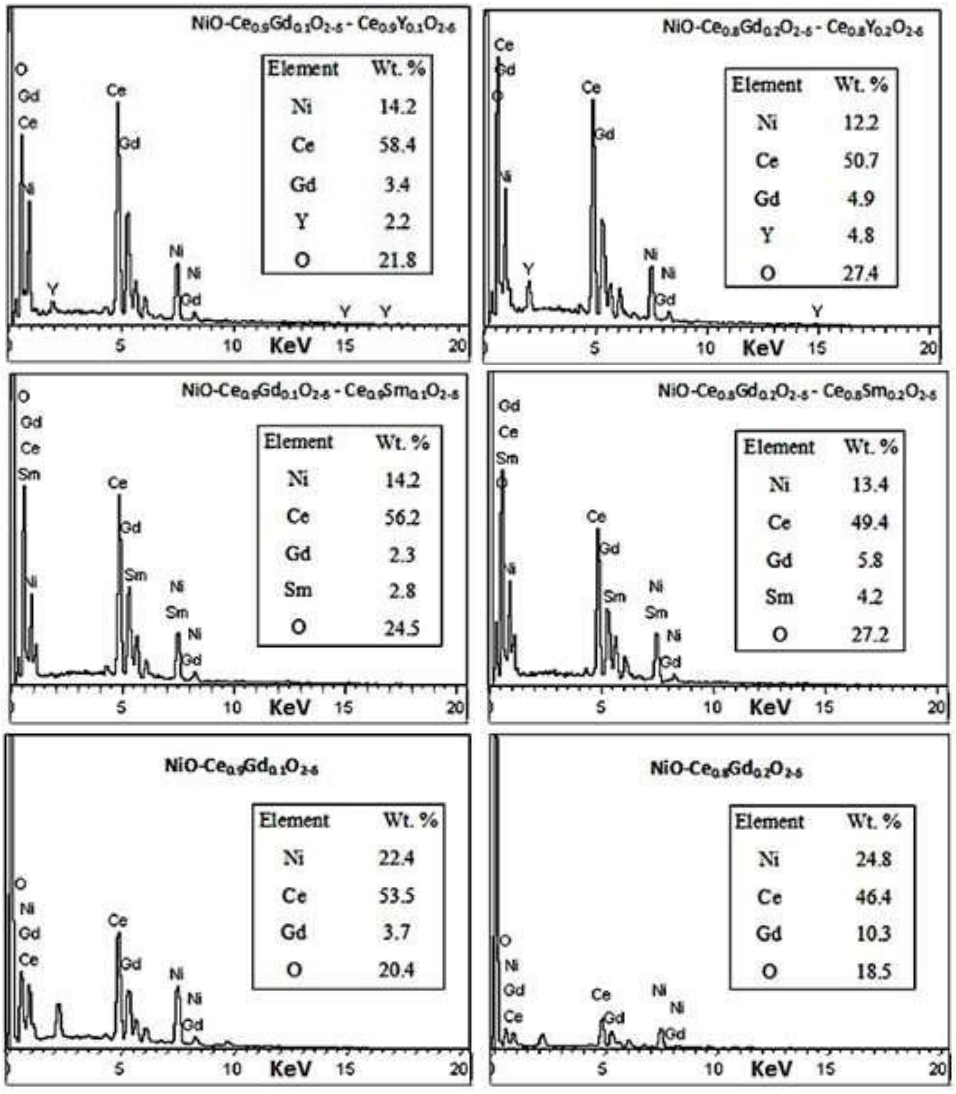


Fig. 12. EDAX spectra obtained on nanocrystalline ceramic composite oxide powders

Table 7. Elemental composition data obtained with nanocrystalline ceramic composite oxide powders prepared by chemical precipitation method

| Sample | Atomic weight percentage (%) | | | | | |
|---|---|---|---|---|---|---|
| | Ce | Gd | Y | Sm | Ni | O |
| NiO-$Ce_{0.9}Gd_{0.1}O_{2-\delta}$-$Ce_{0.9}Y_{0.1}O_{2-\delta}$ | 58.4 | 3.4 | 2.2 | --- | 14.2 | 21.8 |
| NiO-$Ce_{0.8}Gd_{0.2}O_{2-\delta}$ -$Ce_{0.8}Y_{0.2}O_{2-\delta}$ | 50.7 | 4.9 | 4.8 | --- | 12.2 | 27.4 |
| NiO-$Ce_{0.9}Gd_{0.1}O_{2-\delta}$-$Ce_{0.9}Sm_{0.1}O_{2-\delta}$ | 56.2 | 2.3 | --- | 2.8 | 14.2 | 24.5 |
| NiO-$Ce_{0.8}Gd_{0.2}O_{2-\delta}$ -$Ce_{0.8}Sm_{0.2}O_{2-\delta}$ | 49.4 | 5.8 | --- | 4.2 | 13.4 | 27.2 |
| NiO-$Ce_{0.9}Gd_{0.1}O_{2-\delta}$ | 53.5 | 3.7 | --- | --- | 22.4 | 20.4 |
| NiO-$Ce_{0.8}Gd_{0.2}O_{2-\delta}$ | 46.4 | 10.3 | --- | --- | 24.8 | 18.5 |

Fig. 13. Sintered NiO-based nanocrystalline ceramic composite oxide pellet

details mentioned below.

*Sample preparation*

NiO-based nanocrystalline ceramic composite oxide powders were finely ground with the addition of 2-3 drops of binding agent poly ethylene glycol (PEG). They allowed to dry at 50-100 °C for 10-15 minutes. This mixture was subjected to made the circular compacts (with 2 mm thickness and 10 mm diameter) by applying a pressure of 1.2 ton with hydraulic pressure pelletizer. The pellets were sintered at 750 °C for 3 hours in air. The final pellets were obtained with gray color after sintering as shown in Fig. 13. After sintering, the porosity of the pellets became highly dense. These pellets were subjected to high temperature impedance spectroscopy studies in air.

*Electrochemical impedance measurements*

The impedance measurements were carried out different temperatures, such as, room temperature, 300, 400, 500 and 600 °C for all the specimens. The conditions maintained for the analysis of the sample are: 1.3 volts; frequency range 42 Hz to 5 KHz. The impedance curves obtained on the ceria doped nanocrystalline pellets are shown in the Figs. 15-20. Fitting of the measurement data was performed with

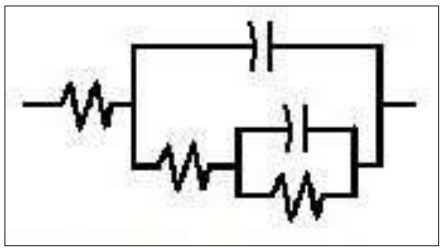

Fig. 14. Equivalent circuit used to fit measurement data obtained on NiO-based nanocrystalline ceramic composite oxide pellets (2RQR) (where, the symbol —|| referred as capacitor (constant phase element, CPE) and the —/\/\— referred as resistor).

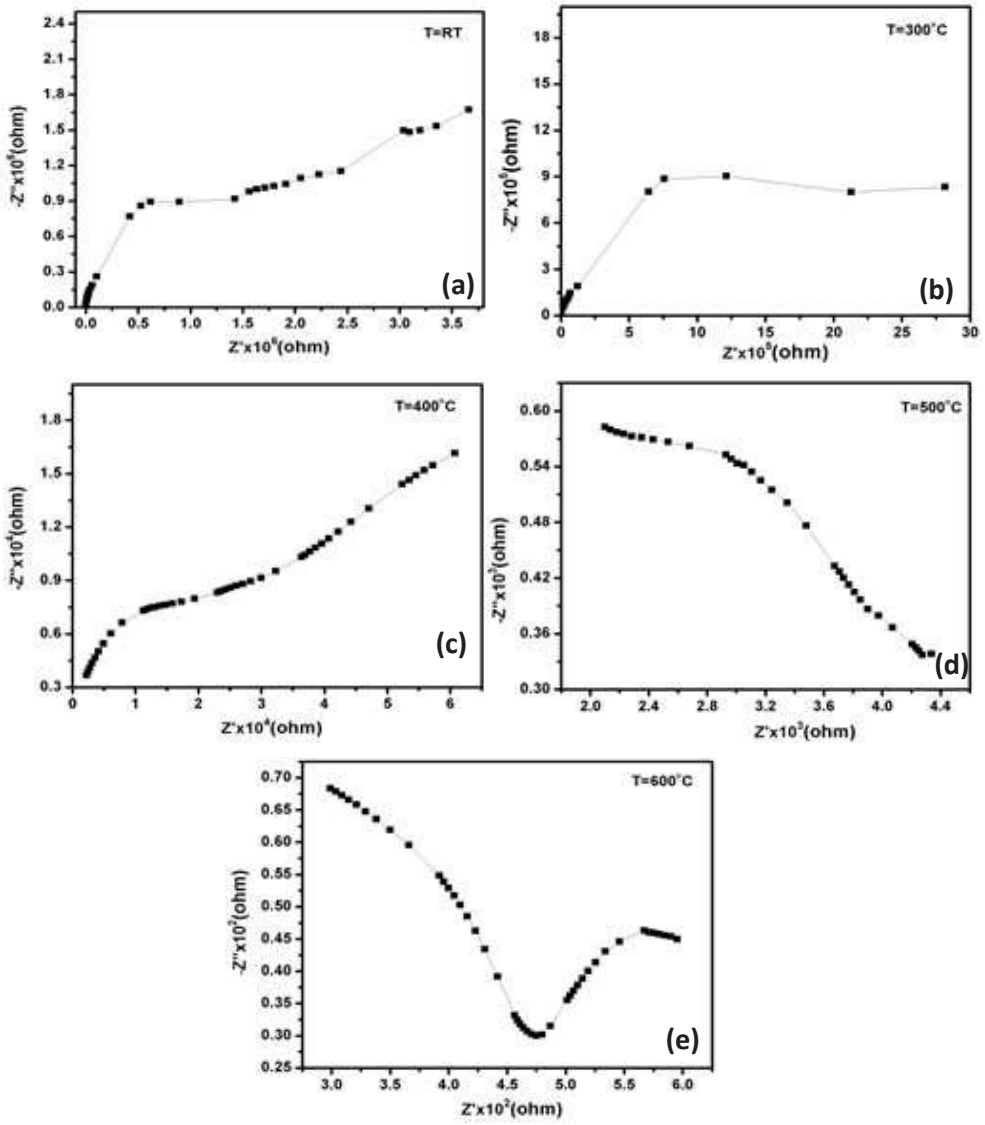


Fig. 15. (a-e) Impedance curves obtained on sintered circular compact of NiO-$Ce_{0.9}Gd_{0.1}O_{2-\delta}$ –$Ce_{0.9}Y_{0.1}O_{2-\delta}$ at different temperatures

the software ZSimpwin of version 3.20. The impedance data of the NiO based nanocrystalline sintered pellets was fitted with the equivalent circuit R(C(R(CR)) as shown in Fig. 14. The impedance spectra was fitted to the conventional equivalent electronic circuit containing three Resistance- Constant Phase Element (R-CPE) sub circuits in series, which generates three semicircles on the Nyquist plots. Equivalent circuit modeling has been accepted as the means of interpreting electrochemical impedance results [42], as this offers a convenient way of analyzing and investigating changes in cell behavior. The semicircle corresponding to the bulk conductivity is lost from the spectrum above 350 °C. At higher temperatures, around 500 °C, the grain boundary semicircle is also lost. This is caused by the effect on the spectra of inductances generated within the experimental apparatus.

The electrical conduction of ceria based materials results from impurity and intrinsic factors. At low temperatures, its conduction is dominated by the dissociated electron concentration from the energy gap of the impurity, whose activation energy of electrical conduction is much lower than that of the intrinsic conduction.

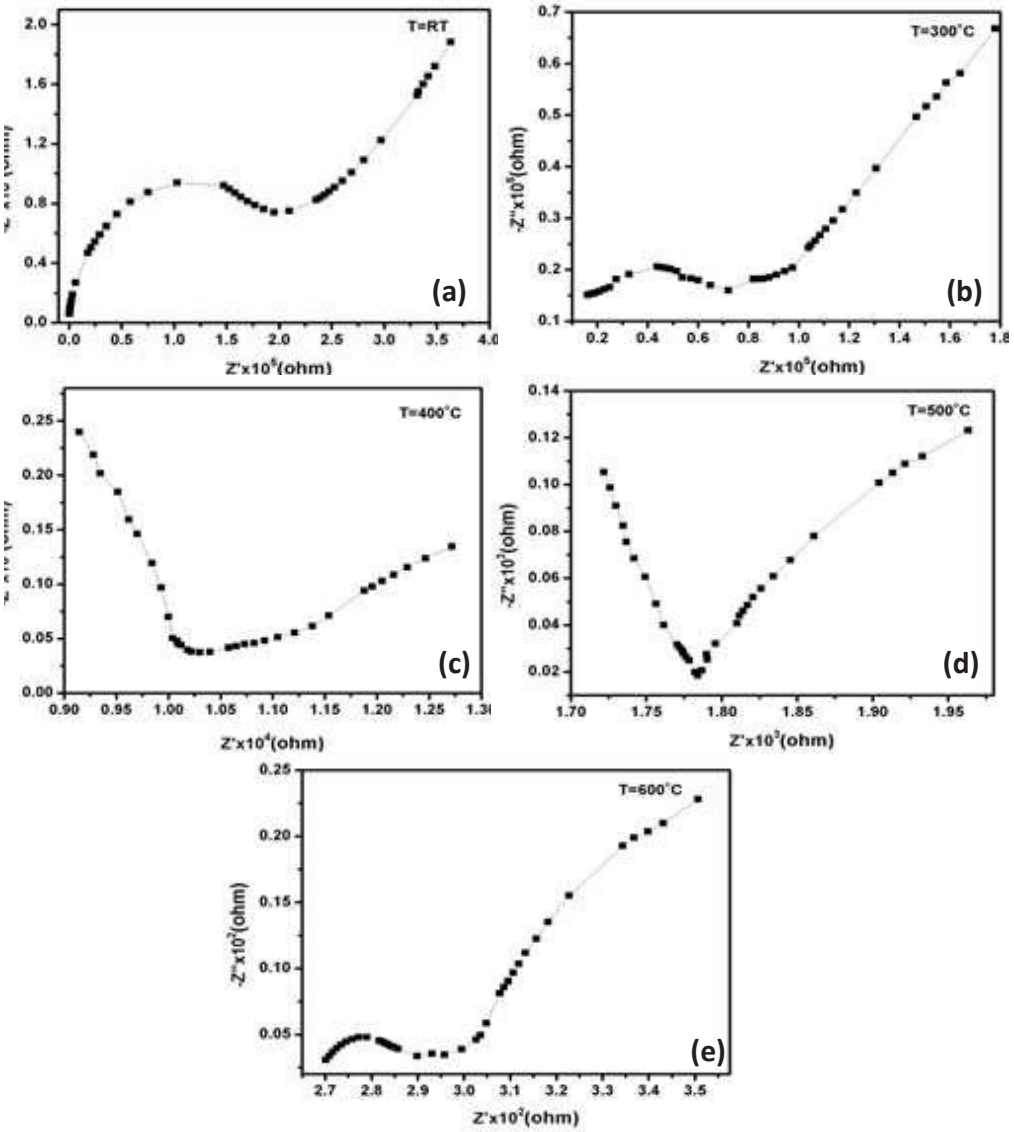


Fig. 16. (a-e) Impedance curves obtained on sintered circular compact of NiO-$Ce_{0.8}Gd_{0.2}O_{2-\delta}$-$Ce_{0.8}Y_{0.2}O_{2-\delta}$ at different temperatures

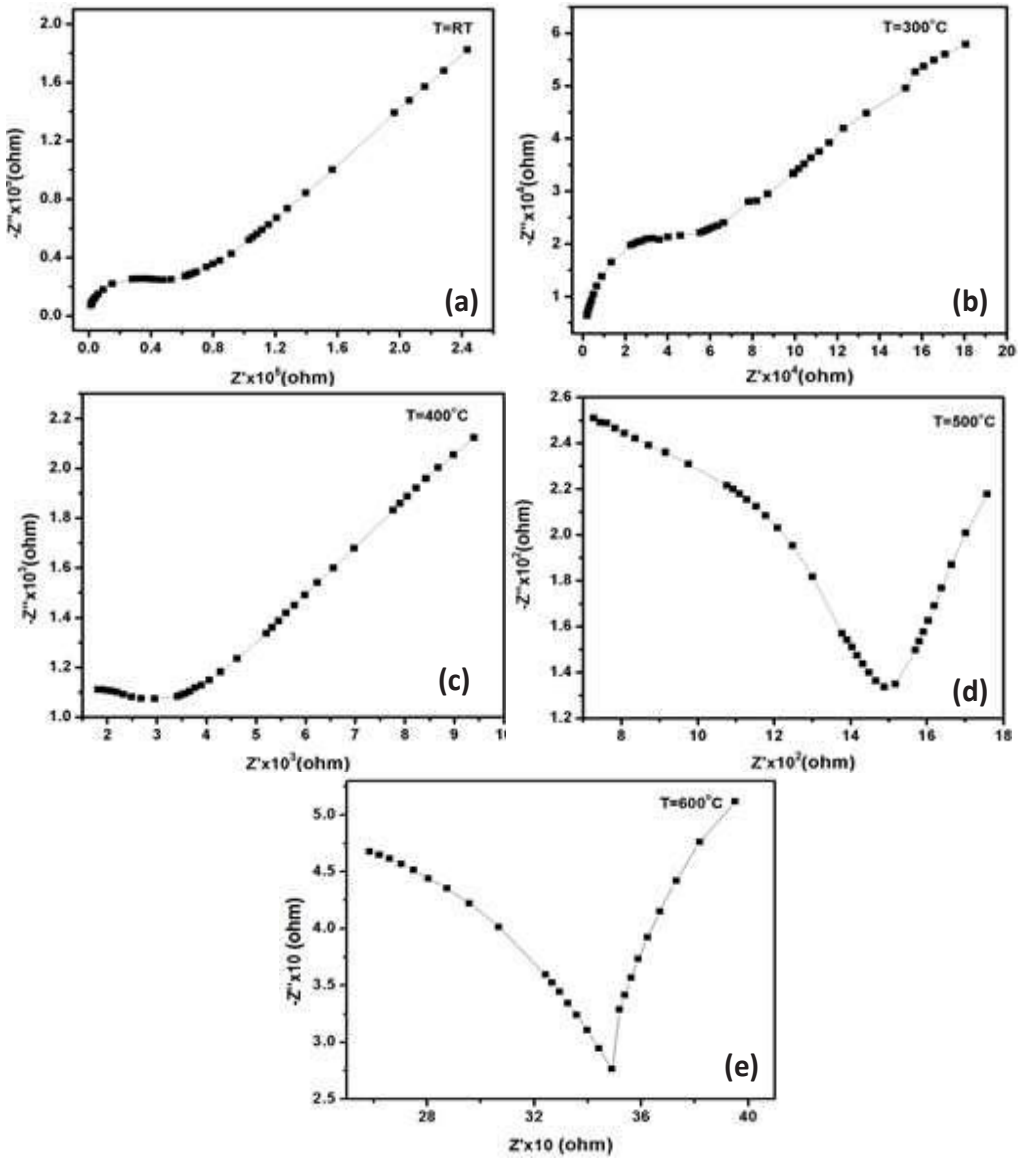


Fig. 17. (a-e) Impedance curves obtained on sintered circular compacts of NiO-$Ce_{0.9}Gd_{0.1}O_{2-\delta}$ –$Ce_{0.9}Sm_{0.1}O_{2-\delta}$ at different temperatures

At high temperatures, the conductivity increase is predominantly due to the intrinsic factor, while electrons from the energy gap of the impurity are all dissociated and activated. The impedance curves obtained on sintered circular compacts of NiO-based nanocrystalline ceramic composite oxide pellets are indicated in Figs. 15-20. The bulk resistance ($R_b$) can be determined from the intercept of the low-frequency part of the arc with real Z'-axis. As the temperature increases, the $R_b$ value shifts towards a lower impedance value. The bulk conductivity can be obtained from the following equation. (Equation 3).

$$\sigma = \frac{t}{RA} \tag{3}$$

Where 'σ' is represented as total conductivity, 't' and 'A' are the thickness and cross sectional area of the pellet and 'R' is a resistance. Conductivity values calculated for sintered nanocrystalline ceramic composite oxide pellets at different temperatures as shown in Table 8.

From the data, it is observed that NiO-$Ce_{0.9}Gd_{0.1}O_{2-\delta}$ exhibited the highest value of

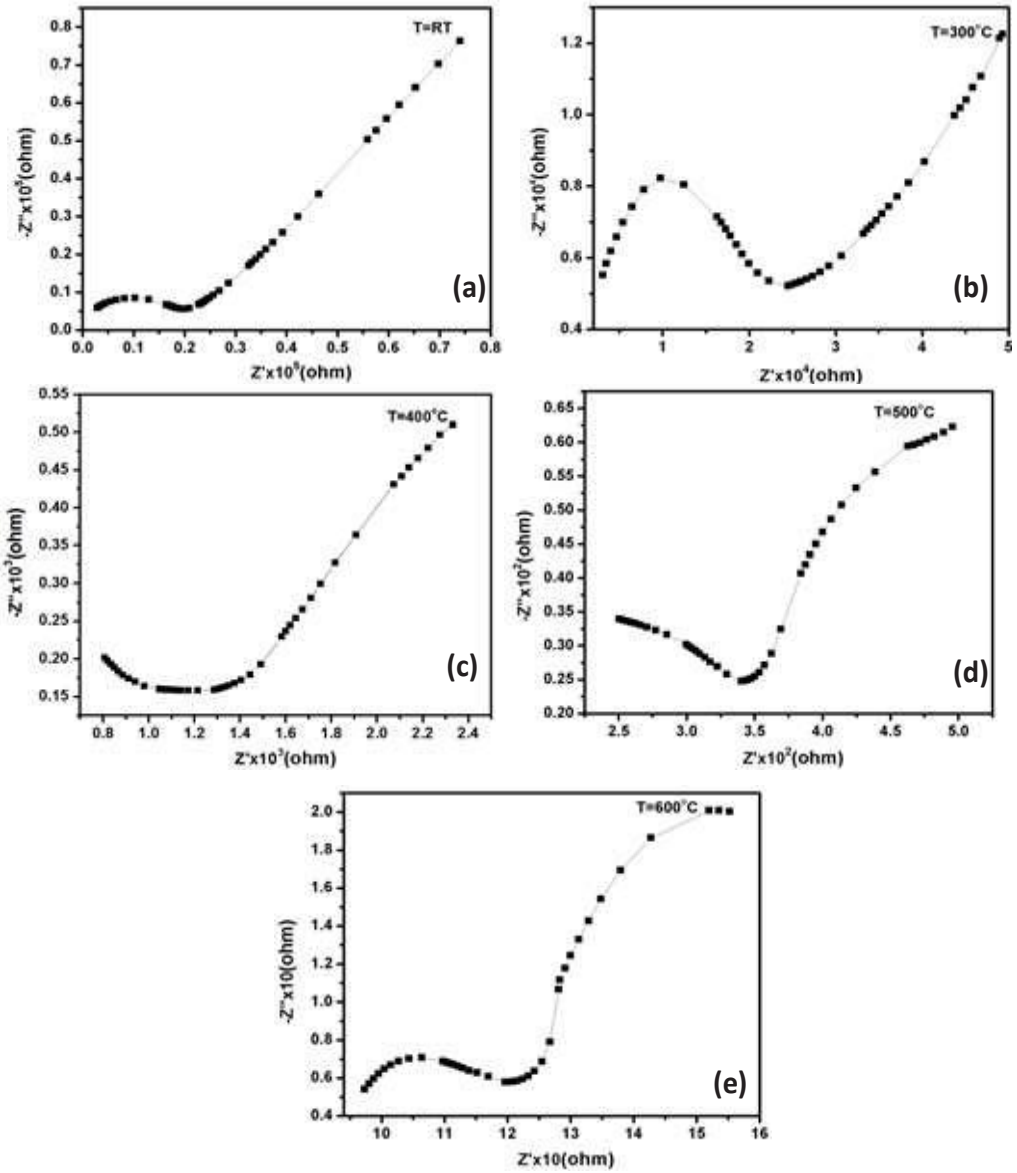


Fig. 18. (a-e) Impedance curves obtained on sintered circular compacts of NiO-$Ce_{0.8}Gd_{0.2}O_{2-\delta}$–$Ce_{0.8}Sm_{0.2}O_{2-\delta}$ at different temperatures

conductivity at 600 °C (8.0544 × $10^{-04}$ $Scm^{-1}$). Petrovsky et al. prepared a novel Y- doped $ZrO_2$ for application in ITSOFC and its electrical conductivity at 700 °C was 0.1 $Scm^{-1}$ in air and >100 $Scm^{-1}$ in reducing atmosphere [43].

The activation energies of all materials have been calculated by using Arrhenius linear fit relationship equation. Activation energies, correspond to the conductivity in high temperature range, were determined from the linear fit of the Arrhenius curves. Activation energy of all samples was calculated by using Arrhenius relationship equation (Equation 4).

$$\sigma_{dc}(T) = \sigma_o \exp(-E_a/K_B T) \quad (5)$$

'σ' is represented as direct current conductivity
T = temperature
$\sigma_o$ = Pre-exponentional factor
$E_a$ = activation energy and
$K_B$= Boltzmann constant

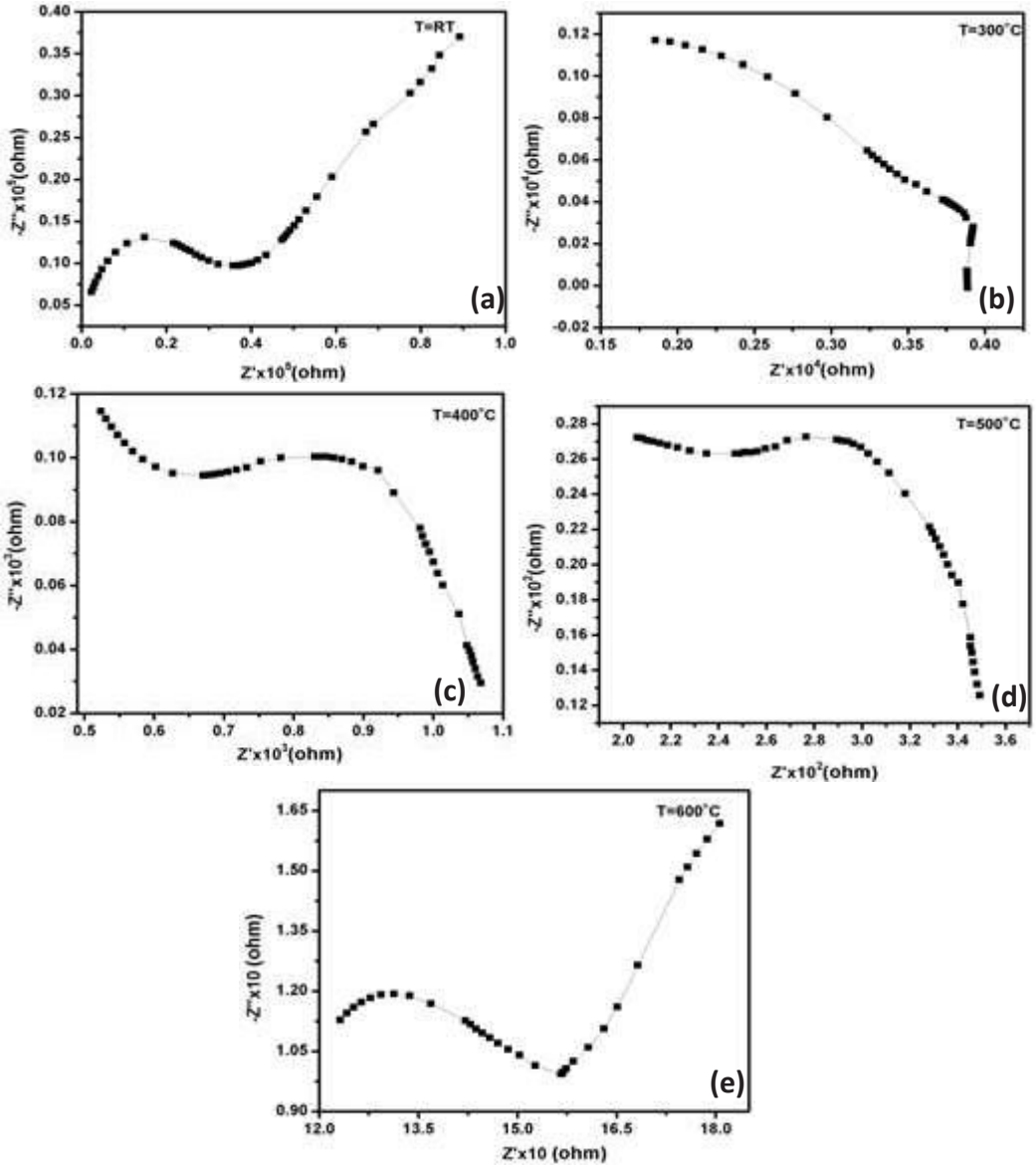


Fig. 19. (a-e) Impedance curves obtained on sintered circular compacts of NiO-$Ce_{0.9}Gd_{0.1}O_{2-\delta}$ at different temperatures

The activation energy values calculated for our samples are shown in Table 9. From the data, it was found that with the increase in the conductivity, the activation energy values were also increased.

Arrhenius-type plots of total conductivity derived from these impedance spectra are presented in Fig. 20 for all anode nanoceramic composite materials. In general, the conductivity was higher for the material sintered at high temperature. Also, there is a decrease in conductivity in all samples as a function of time at 400 and 500 °C. The conductivity values obtained in the samples are found to be less than the reported data because the samples were sintered at temperatures less than the reported data. Hence, it is inferred that by increasing the sintering temperature of the circular anode compacts, the conductivity values may further enhance. The conductivity of anode materials for SOFC can be improved well by sintering them at high temperature for prolonged duration. This will improve the microstructural characteristics of anodes which may result in high electronic conductivity [44].

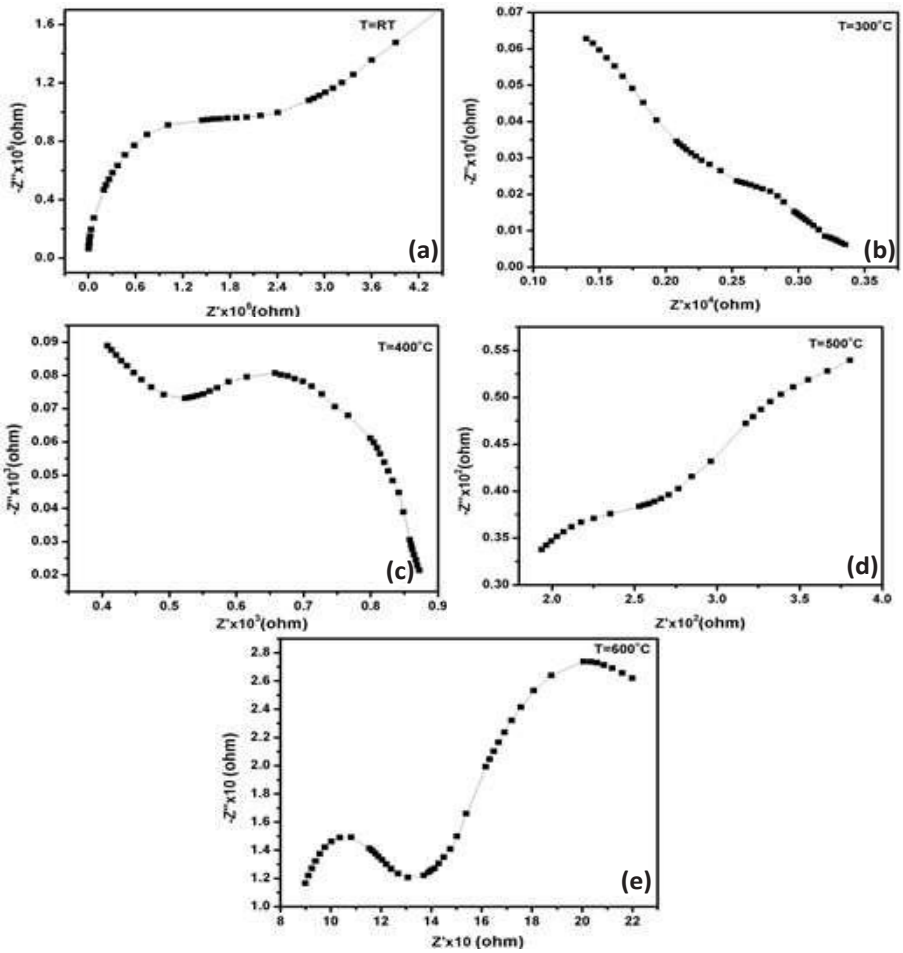


Fig. 20. (a-e) Impedance curves obtained on sintered circular compacts of NiO-$Ce_{0.8}Gd_{0.2}O_{2-\delta}$ at different temperatures

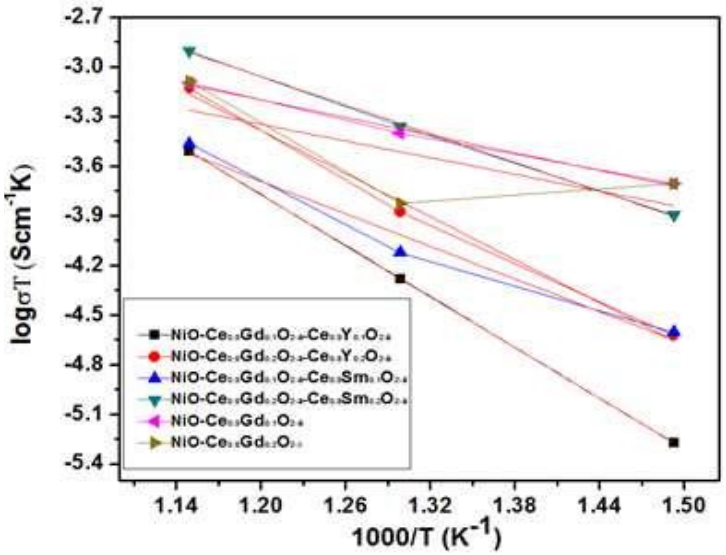


Fig. 21 - Arrhenius linear relationship plot obtained on nanocrystalline ceramic composite oxide pellets

Table 8. Conductivity values calculated for sintered nanocrystalline ceramic composite oxide pellets at different temperatures

| Sample | Electronic conductivity at different temperatures ($Scm^{-1}$) | | | | |
|---|---|---|---|---|---|
| | Room Temperature | 300 °C | 400 °C | 500 °C | 600 °C |
| $NiO\text{-}Ce_{0.9}Gd_{0.1}O_{2-\delta}$-$Ce_{0.9}Y_{0.1}O_{2-\delta}$ | $2.1850 \times 10^{-07}$ | $6.4118 \times 10^{-08}$ | $5.3513 \times 10^{-06}$ | $5.2314 \times 10^{-05}$ | $3.1002 \times 10^{-04}$ |
| $NiO\text{-}Ce_{0.8}Gd_{0.2}O_{2-\delta}$ - $Ce_{0.8}Y_{0.2}O_{2-\delta}$ | $1.0882 \times 10^{-06}$ | $2.4543 \times 10^{-06}$ | $2.3654 \times 10^{-05}$ | $1.3266 \times 10^{-04}$ | $7.4108 \times 10^{-04}$ |
| $NiO\text{-}Ce_{0.9}Gd_{0.1}O_{2-\delta}$-$Ce_{0.9}Sm_{0.1}O_{2-\delta}$ | $2.0265 \times 10^{-06}$ | $2.1694 \times 10^{-06}$ | $2.4895 \times 10^{-05}$ | $7.5263 \times 10^{-05}$ | $3.4358 \times 10^{-04}$ |
| $NiO\text{-}Ce_{0.8}Gd_{0.2}O_{2-\delta}$ - $Ce_{0.8}Sm_{0.2}O_{2-\delta}$ | $7.8151 \times 10^{-06}$ | $7.3273 \times 10^{-06}$ | $1.2710 \times 10^{-04}$ | $4.3843 \times 10^{-04}$ | $1.2501 \times 10^{-03}$ |
| $NiO\text{-}Ce_{0.9}Gd_{0.1}O_{2-\delta}$ | $3.9492 \times 10^{-06}$ | $4.0817 \times 10^{-05}$ | $1.9611 \times 10^{-04}$ | $3.9628 \times 10^{-04}$ | $8.0544 \times 10^{-04}$ |
| $NiO\text{-}Ce_{0.8}Gd_{0.2}O_{2-\delta}$ | $4.3338 \times 10^{-07}$ | $4.6539 \times 10^{-05}$ | $1.9781 \times 10^{-04}$ | $1.5003 \times 10^{-04}$ | $8.1981 \times 10^{-04}$ |

Table 9. Activation energies calculated from Arrhenius linear fit relationship for NiO-based nanocrystalline ceramic composite oxide anodes

| Sample | Temperature (°C) | 1000/T ($K^{-1}$) | log$\sigma$T ($Scm^{-1}K$) | slope | Activation energy (eV) |
|---|---|---|---|---|---|
| $NiO\text{-}Ce_{0.9}Gd_{0.1}O_{2-\delta}$–$Ce_{0.9}Y_{0.1}O_{2-\delta}$ | 400 | 1.492 | -5.271 | | |
| | 500 | 1.298 | -4.281 | - 5.136 | 0.443 |
| | 600 | 1.149 | -3.508 | | |
| $NiO\text{-}Ce_{0.8}Gd_{0.2}O_{2-\delta}$–$Ce_{0.8}Y_{0.2}O_{2-\delta}$ | 400 | 1.492 | -4.626 | | 0.374 |
| | 500 | 1.298 | -3.877 | - 4.335 | |
| | 600 | 1.149 | -3.130 | | |
| $NiO\text{-}Ce_{0.9}Gd_{0.1}O_{2-\delta}$–$Ce_{0.9}Sm_{0.1}O_{2-\delta}$ | 400 | 1.492 | -4.603 | | |
| | 500 | 1.298 | -4.123 | -3.281 | 0.283 |
| | 600 | 1.149 | -3.463 | | |
| $NiO\text{-}Ce_{0.8}Gd_{0.2}O_{2-\delta}$–$Ce_{0.8}Sm_{0.2}O_{2-\delta}$ | 400 | 1.492 | -3.895 | | 0.249 |
| | 500 | 1.298 | -3.358 | -2.887 | |
| | 600 | 1.149 | -2.903 | | |
| $NiO\text{-}Ce_{0.9}Gd_{0.1}O_{2-\delta}$ | 400 | 1.492 | -3.707 | | 0.153 |
| | 500 | 1.298 | -3.401 | -1.778 | |
| | 600 | 1.149 | -3.093 | | |
| $NiO\text{-}Ce_{0.8}Gd_{0.2}O_{2-\delta}$ | 400 | 1.492 | -3.703 | | |
| | 500 | 1.298 | -3.823 | -1.681 | 0.145 |
| | 600 | 1.149 | -3.086 | | |

## CONCLUSIONS

In this research work, a set of nanocrystalline anode materials ($NiO\text{-}Ce_{0.9}Gd_{0.1}O_{2-\delta}$-$Ce_{0.9}Y_{0.1}O_{2-\delta}$, $NiO\text{-}Ce0_{.8}Gd_{0.2}O_{2-\delta}$-$Ce_{0.8}Y_{0.2}O_{2-\delta}$, $NiO\text{-}Ce_{0.9}Gd_{0.1}O_{2-\delta}$-$Ce_{0.9}Sm_{0.1}O_{2-\delta}$, $NiO\text{-}Ce_{0.8}Gd_{0.2}O_{2-\delta}$-$Ce_{0.8}Sm_{0.2}O_{2-\delta}$, $NiO\text{-}Ce_{0.9}Gd_{0.1}O_{2-\delta}$ and $NiO\text{-}Ce_{0.8}Gd_{0.2}O_{2-\delta}$) for SOFC have been successfully developed using a cost-effective facile synthesis, i.e., chemical precipitation method. TGA patterns obtained on the precursor samples revealed the methodology to get phase pure materials. The powder XRD data obtained for all the samples is in agreement with the standard reported JCPDS data. From the FTIR spectra, it was observed that characteristic peak of metal-oxygen bond is present in all the samples. The presence of nano particles was confirmed

by the particle size analysis and SEM. Elemental composition of all the samples was studied by EDAX analysis, which is in accordance with the theoretical data. The conductivity measurements obtained on all the samples revealed that the samples proposed in this research work may be considered as SOFC anodes after sintering them at high temperatures for prolonged duration.

**ACKNOWLEDGMENTS**

ASN would like to thank Central Power Research Institute (Ministry of Power, Govt. of India) (Grant No. CPRI/ R&D/ TC/ GDEC/ 2019, dated 06-02-2019) for financial support. DR and ASN thank Karunya Deemed University for providing necessary facilities in the Department of Chemistry to carry-out this research work.

**CONFLICT OF INTEREST**

The authors declare that there are no conflicts of interest regarding the publication of this manuscript.

**REFERENCES**

1. Gauckler LJ, Beckel D, Buergler BE, Jud E, Muecke UP, Prestat M, et al. Solid Oxide Fuel Cells: Systems and Materials. CHIMIA International Journal for Chemistry. 2004;58(12):837-850.
2. Jo S, Yang J, Park J-Y. Electrochemcial Performances of La-Doped $SrTiO_3$ Anode Materials for Intermediate Temperature-Solid Oxide Fuel Cells. ECS Transactions. 2017;78(1):1237-1243.
3. Wang W, Qu J, Julião PSB, Shao Z. Recent Advances in the Development of Anode Materials for Solid Oxide Fuel Cells Utilizing Liquid Oxygenated Hydrocarbon Fuels: A Mini Review. Energy Technology. 2018;7(1):33-44.
4. Liu C-b, Yu L-s, Jiang X-l. Particle growth mechanism of nanocrystalline zirconia powder during high temperature heat treatment. Transactions of Nonferrous Metals Society of China. 2007;17(5):1022-1027.
5. Li Y, Luo Z-y, Yu C-j, Luo D, Xu Z-a, Cen K-f. The impact of NiO on microstructure and electrical property of solid oxide fuel cell anode. Journal of Zhejiang University Science B. 2005;6(11):1124-1129.
6. Zhu WZ, Deevi SC. A review on the status of anode materials for solid oxide fuel cells. Materials Science and Engineering: A. 2003;362(1-2):228-239.
7. Raza R, Liu Q, Nisar J, Wang X, Ma Y, Zhu B. ZnO/NiO nanocomposite electrodes for low-temperature solid oxide fuel cells. Electrochem Commun. 2011;13(9):917-920.
8. Nai-Tao Y, Yi-Chi S, Wei YAN, Xiu-Xia M, Xiao-Yao TAN, Zi-Feng MA. Microstructure and Performance of Anode for Microtubular Solid Oxide Fuel Cells. Journal of Inorganic Materials. 2014;29(12):1246.
9. Zha S. Ni-Ce0.9Gd0.1O1.95 anode for GDC electrolyte-based low-temperature SOFCs. Solid State Ionics. 2004;166(3-4):241-250.
10. Ghiyasiyan-Arani M, Salavati-Niasari M. Effect of $Li_2CoMn_3O_8$ Nanostructures Synthesized by a Combustion Method on Montmorillonite K10 as a Potential Hydrogen Storage Material. The Journal of Physical Chemistry C. 2018;122(29):16498-16509.
11. Salehabadi A, Sarrami F, Salavati-Niasari M, Gholami T, Spagnoli D, Karton A. $Dy_3Al_2(AlO_4)_3$ ceramic nanogarnets: Sol-gel auto-combustion synthesis, characterization and joint experimental and computational structural analysis for electrochemical hydrogen storage performances. J Alloys Compd. 2018;744:574-582.
12. Mazloom F, Ghiyasiyan-Arani M, Monsef R, Salavati-Niasari M. Photocatalytic degradation of diverse organic dyes by sol–gel synthesized $Cd_2V_2O_7$ nanostructures. Journal of Materials Science: Materials in Electronics. 2018;29(21):18120-18127.
13. Monsef R, Ghiyasiyan-Arani M, Salavati-Niasari M. Utilizing of neodymium vanadate nanoparticles as an efficient catalyst to boost the photocatalytic water purification. J Environ Manage. 2019;230:266-281.
14. Namvar F, Sadat Sangsefidi F, Salavati-Niasari M. Tb2MoO6 nanostructure: Ultrasonic controlling the size and morphology, characterization and investigation of its photo-catalytic activity for dyes as the water pollutants under UV light illumination. J Hazard Mater. 2018;360:288-302.
15. Haghjoo H, Sangsefidi FS, Salavati-Niasari M. Synthesis and characterization of $Pb_2SiO_4$ nanostructure: study of photo-catalytic behavior of reactive Red198 and reactive Orange16 dyes as pollutants. Journal of Materials Science: Materials in Electronics. 2018;29(10):8002-8009.
16. Haghjoo H, Sangsefidi FS, Hashemizadeh SA, Salavati-Niasari M. Investigation the magnetic properties and the photocatalytic activity of synthesized Mn 7 SiO 12 nanostructures by green capping agent. J Mol Liq. 2017;225:290-295.
17. Haghjoo H, Sangsefidi FS, Salavati-Niasari M. Study on the optical, magnetic, and photocatalytic activities of the synthesized $Mn_2O_3$-$SiO_2$ nanocomposites by microwave method. J Mol Liq. 2017;242:779-788.
18. Haghjoo H, Sangsefidi FS, Salavati-Niasari M. Synthesis of $PbSiO_3$ nanoparticles in the presence of proteins as a greencapping agent and their application as photocatalyst. J Mol Liq. 2017;247:345-353.
19. Sangsefidi FS, Sabet M, Salavati-Niasari M. Synthesis and characterization of ceria nanostructures with different morphologies via a simple thermal decompose method with different cerium complexes and investigation the photocatalytic activity. Journal of Materials Science: Materials in Electronics. 2016;27(8):8793-8801.
20. Sangsefidi FS, Salavati-Niasari M, Khojasteh H, Shabani-Nooshabadi M. Synthesis, characterization and investigation of the electrochemical hydrogen storage properties of CuO–$CeO_2$ nanocomposites synthesized by green method. Int J Hydrogen Energy. 2017;42(21):14608-14620.
21. Sangsefidi FS, Salavati-Niasari M, Varshoy S, Shabani-Nooshabadi M. Investigation of $Mn_2O_3$ as impurity on the electrochemical hydrogen storage performance of $MnO_2CeO_2$ nanocomposites. Int J Hydrogen Energy. 2017;42(47):28473-28484.
22. Sangsefidi FS, Salavati-Niasari M. Thermal decomposition synthesis, characterization and electrochemical

hydrogen storage characteristics of $Co_3O_4$–$CeO_2$ porous nanocomposite. Int J Hydrogen Energy. 2017;42(31):20071-20081.
23. Sangsefidi FS, Salavati-Niasari M, Mazaheri S, Sabet M. Controlled green synthesis and characterization of $CeO_2$ nanostructures as materials for the determination of ascorbic acid. J Mol Liq. 2017;241:772-781.
24. Sangsefidi FS, Nejati M, Verdi J, Salavati-Niasari M. Green synthesis and characterization of cerium oxide nanostructures in the presence carbohydrate sugars as a capping agent and investigation of their cytotoxicity on the mesenchymal stem cell. Journal of Cleaner Production. 2017;156:741-749.
25. Sangsefidi FS, Salavati-Niasari M. $Fe_2O_3$–$CeO_2$ Ceramic Nanocomposite Oxide: Characterization and Investigation of the Effect of Morphology on Its Electrochemical Hydrogen Storage Capacity. ACS Applied Energy Materials. 2018;1(9):4840-4848.
26. Sangsefidi FS, Salavati-Niasari M, Shabani-Nooshabadi M. Characterization of hydrogen storage behavior of the as-synthesized p-type NiO/n-type $CeO_2$ nanocomposites by carbohydrates as a capping agent: The influence of morphology. Int J Hydrogen Energy. 2018;43(31):14557-14568.
27. Sangsefidi FS, Salavati-Niasari M, Ghasemifard M, Shabani-Nooshabadi M. Study of hydrogen storage performance of ZnO–$CeO_2$ ceramic nanocomposite and the effect of various parameters to reach the optimum product. Int J Hydrogen Energy. 2018;43(51):22955-22965.
28. Ketzial JSSJ, Radhika D, Nesaraj AS. Low-temperature preparation and physical characterization of doped $BaCeO_3$ nanoparticles by chemical precipitation. International Journal of Industrial Chemistry. 2013;4(1):18.
29. Song X, Jiang N, Li Y, Xu D, Qiu G. Synthesis and Characterization of Y-Doped Mesoporous $CeO_2$ Using A Chemical Precipitation Method. Journal of Rare Earths. 2007;25(4):428-433.
30. Bahari Molla Mahaleh Y, Sadrnezhaad SK, Hosseini D. NiO Nanoparticles Synthesis by Chemical Precipitation and Effect of Applied Surfactant on Distribution of Particle Size. Journal of Nanomaterials. 2008;2008:1-4.
31. Thomassen L. An X-Ray Investigation of the System $Cr_2O_3$-$NiO_1$. J Am Chem Soc. 1940;62(5):1134-1136.
32. Wołcyrz M, Kepinski L. Rietveld refinement of the structure of CeOCl formed in Pd/$CeO_2$ catalyst: Notes on the existence of a stabilized tetragonal phase of $La_2O_3$ in LaPdO system. J Solid State Chem. 1992;99(2):409-413.
33. Fuentes R, Baker R. Synthesis and properties of Gadolinium-doped ceria solid solutions for IT-SOFC electrolytes. Int J Hydrogen Energy. 2008;33(13):3480-3484.
34. Guan X, Zhou H, Liu Z, Wang Y, Zhang J. High performance $Gd^{3+}$ and $Y^{3+}$ co-doped ceria-based electrolytes for intermediate temperature solid oxide fuel cells. Mater Res Bull. 2008;43(4):1046-1054.
35. Tao Y, Shao J, Wang J, Wang WG. Morphology control of $Ce_{0.9}Gd_{0.1}O_{1.95}$ nanopowder synthesized by sol–gel method using PVP as a surfactant. J Alloys Compd. 2009;484(1-2):729-733.
36. Bhatt AS, Bhat DK, Santosh MS, Tai C-w. Chitosan/NiO nanocomposites: a potential new dielectric material. J Mater Chem. 2011;21(35):13490.
37. Jasmine Ketzial J, Samson Nesaraj A, Synthesis of $CeO_2$ nanoparticles by chemical precipitation and the effect of a surfactant on the distribution of particle sizes. J Ceram Process Res., 2011, 12(1): pp. 74-79.
38. Tas A C, Majewski P J, Aldinger F, Chemical preparation of pure and strontium- and/or magnesium-doped lanthanum gallate powders. J Am Ceram Soc., 2000; 83 (12):2954-2960.
39. Subramanya Herle P, Hegde M S, Subbanna G N, Synthesis and structure of a new oxynitride $Ba_3W_2O_6N_2$. J Mater Chem., 1997; 7 (10): 2121-2125.
40. Liu C, Yu L, Jiang X, Particle growth mechanism of nanocrystalline zirconia powder during high temperature heat treatment. T Nonferr Metal Soc., 2007; 17(5): 1022 – 1027.
41. Eguchi K, Setoguchi T, Inoue T, Arai H, "Electrical properties of ceria-based oxides and their application to solid oxide fuel cells" Solid State Ionics, 1992; 52: 165–172.
42. Macdonald J R, Franceschetti D R, Precision of impedance spectroscopy estimates of bulk, reaction rate, and diffusion parameters. J. Electroanal. Chem. Interf. Electrochem., 1991; 307(1-2):1-11.
43. Petrovsky V, Suzuki T, Jasinski P, Anderson H U, Low-temperature processed anode for solid oxide fuel cells. Electrochem Solid St, 2005; 8(7): A341-A343.
44. Liu T, Ren C, Fang S, Wang Y, Chen F. Microstructure tailoring of the nickel oxide–yttria-stabilized zirconia hollow fibers toward high-performance microtubular solid oxide fuel cells. ACS Appl Mater Interfaces. 2014;6(21):18853-8860.